Phosphorylation of an Arabidopsis villin activates host actin remodeling to restrict microbial invasion

Minxia Zou
Beijing Normal University
Mengmeng Guo
Beijing Normal University
Zhaoyang Zhou
China Agriculture University
Bingxiao Xiao
Beijing Normal University
Qing Pan
Beijing Normal University
Jiajing Li
Beijing Normal University
Jian-Min Zhou
Institute of Genetics and Developmental Biology, Academy of Seed Design, Chinese Academy of Sciences https://orcid.org/0000-0002-9943-2975
Jiejie Li (jiejieli@bnu.edu.cn)
Beijing Normal University

Article

Keywords: Actin Cytoskeleton, Cytoplasmic Filaments, Incessant Turnover Mechanisms, Innate Immunity Gates, Phosphorylation Assays

Posted Date: January 6th, 2021

DOI: https://doi.org/10.21203/rs.3.rs-139790/v1

Version of Record: A version of this preprint was published at Nature Communications on November 9th, 2021. See the published version at https://doi.org/10.1038/s41467-021-26827-2.

Phosphorylation of an Arabidopsis villin activates host actin remodeling to restrict microbial invasion

Minxia Zou[1], Mengmeng Guo[1], Zhaoyang Zhou[4], Bingxiao Wang[1], Qing Pan[1], Jiajing Li[1], Jian-Min Zhou[3,5] and Jiejie Li[1,2*]

[1] Beijing Key Laboratory of Gene Resource and Molecular Development, College of Life Science, Beijing Normal University, Beijing, 100875, China

[2] Key Laboratory of Cell Proliferation and Regulation of Ministry of Education, College of Life Science, Beijing Normal University, Beijing, 100875, China

[3] State Key Laboratory of Plant Genomics, Institute of Genetics and Developmental Biology, Innovation Academy for Seed Design, Chinese Academy of Sciences, Beijing, 100101, China

[4] Department of Vegetable Sciences, Beijing Key Laboratory of Growth and Developmental Regulation for Protected Vegetable Crops, China Agricultural University, Beijing, 100193, China

[5] CAS Center for Excellence in Biotic Interactions, University of Chinese Academy of Sciences, Beijing 100049, China

Abstract

Actin cytoskeleton is a dynamic framework of cytoplasmic filaments that rearranges as the needs of the cell change during growth and development. Incessant turnover mechanisms allow these networks to be rapidly redeployed in defense of host cytoplasm against microbial invaders. However, the precise functions of host actin and the molecular mechanisms underlying actin rearrangements in host defense remain largely unknown. Here, we uncover the mechanism by which host actin controls innate immunity gates on plant surface to actively prevent microbial entry into internal tissue. VLN3, a villin protein from *Arabidopsis* is a key regulator of this process. Our *in vitro* and *in vivo* phosphorylation assays show that VLN3 is a physiological substrate of two pathogen-responsive mitogen-activated protein kinases (MAPKs). Quantitative analyses of actin dynamics and genetic studies reveal that phosphorylation of VLN3 by MAPKs govern actin remodeling to activate innate immunity gating on host surface.

Introduction

Innate immunity is characterized by the rapid and nonspecific responses to invading pathogens. Activation of plant and animal innate immunity requires the recognition of microbe-associated molecular patterns (MAMPs) by cell surface receptors. Immune responses in plants, known as pattern-triggered immunity (PTI), include activation of mitogen-associated and calcium-dependent protein kinases (MAPK and CDPK), bursts of cytosolic calcium and reactive oxygen species (ROS), production of defense hormones such as salicylic acid, and activation/inhibition of ion channels[1]. These signaling events ensure robust defense responses to abrogate the pathogen infection.

Actin cytoskeleton is a dynamic framework of cytoplasmic filaments that rearranges as the needs of the cell change during growth and development[2]. Increasing evidence points to the importance of actin cytoskeleton for innate immunity in both plants and animals[3]. In mammalian cells, Toll-like receptors perceive MAMPs to trigger dynamic cellular changes to resist pathogen attack, which often depend on actin remodeling to rearrange receptors and cell-signaling intermediates, and to mediate membrane movements in processes such as endocytosis, plasma membrane ruffling and phagocytosis[4]. In plant cells, actin remodeling has often been observed in response to a variety of plant-microbe interactions[3]. A rapid increase in actin filament abundance occurs within minutes upon receptor activation in Arabidopsis epidermal cells, and this is considered as a novel early hallmark of PTI responses. Many defense responses, such as ligand-induced endocytosis of receptors, organelle rearrangements and targeted delivery of defense compounds to the infection site, are dependent on actin remodeling. Furthermore, cell wall fortification by callose deposition, apoplastic ROS production, as well as transcriptional reprogramming of defense genes is significantly impaired when the host actin cytoskeleton is disrupted. Thus, actin remodeling and associated cellular processes are important for organizing intracellular and apoplastic defenses in host plants; when the actin cytoskeleton is perturbed, plants are more susceptible to both pathogenic and nonpathogenic microbes[3]. Actin cytoskeleton is not only a key target of innate immune signaling in perception of microbes but also integrates the signaling to further elicit broad cytological defense responses. However, the precise functions of host actin cytoskeleton and the molecular mechanisms underlying actin rearrangements in host defense remain poorly understood.

Many actin-binding proteins (ABPs) can sense intracellular secondary messengers such as Ca^{2+}, phospholipids, ROS and pH and are modulated through posttranslational modifications (PTMs) such as phosphorylation or oxidation. ABPs are excellent candidates for transducing signals into cytoskeletal remodeling. Several ABPs have been shown to perceive early hallmarks of defense signaling and alter actin cytoskeletal dynamics to regulate defense[3]. Phosphatidic acid (PA) and ROS generated upon immunity activation inhibit the barbed-end capping activity of capping protein (CP)[5, 6]. Porter et al (2012) suggest that actin depolymerizing factor 4 (ADF4) is phosphorylated during plant defense response. This phosphorylation negatively regulates actin binding, and appears to be important for plant disease symptoms and hypersensitive response phenotype[7]. A very recent study reported that CPK3 phosphorylates ADF4 to regulate actin dynamics in response to MAMP and bacterial treatment. CPK3-mediated actin remodeling is important for plant resistance to bacterial infection[8]. In addition, quantitative phosphoproteomic analyses in *Arabidopsis* suggest that multiple cytoskeletal proteins are rapidly phosphorylated upon treatment with bacterial flagellin peptide mimic flg22. Several phospho-peptides from an Arabidopsis villin isovariant, villin3 (VLN3) have been reported[9, 10]. A follow-up study further indicated that VLN3 is a potential MAPK substrate[10, 11]. These studies suggest a role of VLN3 in plant innate immunity.

VLN3 belongs to the villin/gelsolin/fragmin superfamily, whose members are multifunctional proteins that are widely expressed in most eukaryotic cells[12]. The *Arabidopsis* genome encodes five isovariants of villin, VLN1 to VLN5. They are abundantly expressed in a wide range of tissues, with elevated expression levels in certain types of cells[13]. Except for VLN1, Arabidopsis villins exhibit actin filament bundling, Ca^{2+}-dependent severing and barbed end capping activities[14–17]. VLN3, together with its closest homologue VLN2, regulates actin bundle formation in cortical actin array, which is required for directional organ grown[17, 18]. In this study, we show that host actin not only organizes intracellular and apoplastic defenses, but also controls innate immunity gates on plant surface to actively prevent bacteria from entering the interior space. We uncovered the mechanism by which VLN3-dependent actin rearrangements modulates PTI-induced guard cell gating. Moreover, VLN3 is phosphorylated by two key pathogen-responsive kinases. Phosphorylation of VLN3 activates actin remodeling to limit bacterial infection on host surface.

Results

Arabidopsis VLN3 plays an essential role in stomatal immunity

Phosphoproteomic analyses show that VLN3 is phosphorylated upon MAMP activation[9], this promotes us to hypothesize that VLN3 is required for plant immunity. To test this, we inoculated homozygous loss of function *vln3-1* and *vln3-2* mutants with bacterial pathogen *P. syringae* pv. *tomato DC3000* (DC3000). As shown in Figure 1, when inoculated by hand infiltration of rosette leaves, both mutants showed enhanced susceptibility to DC3000 compared with wild-type (WT) plants. In experiments using spray-inoculation, the *vln3* mutants supported significantly greater growth of bacteria (Figure 1A, B). We also accessed the involvement of VLN2, the closest homolog of VLN3, in plant defense to pathogens (Supplemental Figure 1A). The single *vln2-1* mutant was not significantly different from WT when spray-inoculated with DC3000. Moreover, a *vln2vln3* mutant did not show enhanced disease symptoms compared to *vln3* single mutant (Supplemental Figure 1A), suggesting a dominate role of VLN3 in plant immunity. The differences in bacterial growth between two types of inoculation suggest an involvement of plant stomatal defense. Microbial entry into host tissues is the first step of infection in animals and plants. Most plant pathogens can gain entry through nature openings such as stomata pores. In *Arabidopsis*, it has been shown that stomata close upon bacterial infection. This control of stomatal closure is known as stomatal immunity[19]. The restrictive role of stomatal closure on bacteria proliferation was more effective against bacteria inoculated onto the leaf surface than ones artificially infiltrated into the intercellular spaces[19]. Thus, the greater growth of DC3000 strain on *vln3* mutants infected by spray-inoculation (Figure 1A), compared with hand infiltration (Figure 1B), suggests that VLN3 play a role in stomatal defense.

The stomatal movements following treatments with DC3000 and flg22 were further examined. Consistent with previous study[19], both bacteria and MAMP trigger stomatal closure in WT plants, whereas stomata in *vln3* mutants were less responsive to these stimuli (Figure 1C-E). Mutants of other villin isovariants (e.g., *vln2-1* and *vln4-1*) showed WT stomatal responses to MAMPs (Supplemental Figure 1B). To investigate whether VLN3 is specifically involved in defense-associated stomatal movement, various treatments were applied. ABA, $CaCl_2$ and dark-induced stomatal closure are not significantly different between WT and *vln3*. Upon treatment with SA and H_2O_2, mutant stomata close less than WT (Supplemental Figure 1C). These observations indicate that VLN3 is required for optimal stomatal closure in response

to multiple factors. The importance of VLN3 in stomatal defense was further confirmed by a pathogen entry assay. This assay assesses the number of bacteria that enter into the apoplastic spaces of leaves in a given period of time[20]. We found that ~10-fold more bacteria entered into mutant leaf interior (Figure 1F), this phenotype was not caused by the differences in stomata number because WT and mutant show similar stomatal density (Figure 1G). To further investigate the role of VLN3 in other PTI responses, we assessed several hallmarks of PTI in *vln3* mutant, including callose deposition, MAPK activation and ROS production. Neither flg22-dependent MAPK activation nor ROS production was altered by loss of VLN3 (Supplemental Figure 1F, G). However, callose deposition was reduced in *vln3* mutants compared to WT (Supplemental Figure 1D, E). Taken together, these data suggest that, in addition to stomatal defense, VLN3 is an essential component for mounting various immune responses in *Arabidopsis*.

VLN3 is phosphorylated by MPK3/MPK6 during innate immunity

To verify VLN3 phosphorylation *in vivo*, truncated VLN3 fragments were expressed in Arabidopsis protoplasts and total protein samples were subjected to phos-tag gel analysis (Figure 2A). In mock-treated cells, both unphosphorylated and phosphorylated VLN3 C-terminus were detected. Upon flg22 treatment, the lower C-VLN3 bands were shifted to a higher molecular weight, which was nearly abolished by the addition of phosphatase. No upshift of N-VLN3 bands were detected with or without the trigger (Figure 2A). These data suggest that VLN3 C terminus is phosphorylated upon PTI activation. VLN3 has been suggested as a potential MAPK substrate[10, 11]. In *Arabidopsis*, MPK3, MPK4, and MPK6 are rapidly activated upon plant perception of MAMPs. They play critical roles in multiple plant defense responses[21]. It was shown that elevated MPK4 activity compromises Arabidopsis resistance to spray-inoculated bacteria, but not bacteria- or flg22-induced stomatal closure[22], whereas MPK3/MPK6 are essential to stomatal immunity[20]. Based on these results, we hypothesize that VLN3 is a substrate of MPK3 and MPK6. To test this hypothesis, we first explored the interaction between VLN3 and MPK3/MPK6 *in vivo*. Split-luciferase (split-LUC) complementation assays in *Nicotiana benthamiana* were performed (Figure 2B). VLN3 was fused to the N terminus of luciferase (VLN3-Nluc), and MPK3/MPK6 was fused to the C terminus of luciferase (MPK3/6-Cluc). The split-LUC assays showed that transient coexpression of VLN3-Nluc and MPK3/6-Cluc in *N.*

benthamiana yielded strong luminescence signals, but no signal was detected when another actin regulator MDP25 and MPK3/6 were coexpressed (Figure 2B). Coimmunoprecipitation assays further confirmed the interaction between VLN3 and MPK3/MPK6 (Figure 2C). Total protein was isolated from *N. benthamiana* leaves expressing the construct *35S:Flag-MPK3/MPK6* and *35S:GFP-VLN3*. MPK3/MPK6 was immunoprecipitated with anti-Flag antibody conjugated agarose, and VLN3 was detected in the pull-down products by anti-GFP antibodies. Flg22 treatment did not obviously alter the interaction between MPK3/MPK6 and VLN3 (Figure 2C). These data suggest that VLN3 interacts with MPK3/MPK6 *in vivo*, and this interaction is independent of flg22 activation.

We next sought to determine if MPK3/MPK6 phosphorylate VLN3. We purified recombinant VLN3 protein and performed *in vitro* kinase assays. As shown in Figure 2D, recombinant His-MPK3 and His-MPK6 strongly phosphorylated C-VLN3 after activation by constitutively active $MKK5^{DD}$. We did not detect the phosphorylation of N-VLN3 by MPK3/MPK6 (Figure 2D). This result suggests that MPK3/MPK6 directly phosphorylate VLN3 *in vitro*. The phosphorylated VLN3 C terminus was subject to mass spectrum analysis to determine phosphorylation sites in VLN3. Multiple amino acid residues were readily identified as residues phosphorylated by both MPK3/MPK6 *in vitro* (Supplemental Figure 2A). After mutating these residues to Ala, we found that mutations in Thr777 or Ser779 completely abolished the flg22-induced VLN3 phosphorylation *in vivo* (Figure 2F; Supplemental Figure 2B). The *in vitro* kinase assays further confirmed that Thr777 and Ser779 are required for the phosphorylation by MPK3/6, supporting that they are MPK3/MPK6 phosphosites (Figure 2E). We next validated whether the phosphorylation of VLN3 by MPK3/MPK6 occurs *in vivo*. As indicated by immunoblot with anti-phospho-Ser/Thr antibodies, VLN3 became strongly phosphorylated after flg22 treatment. Conversely, and in support of our hypothesis, VLN3 phosphorylation was reduced in *mpk3mpk6* double mutants (Figure 2G). Thus, both *in vitro* and *in vivo* phosphorylation assays confirmed that VLN3 is phosphorylated during innate immunity and this phosphorylation requires MPK3 and MPK6. To test if VLN2 are also phosphorylated by MPK3/MPK6, *in vitro* kinase assays were performed. We did not detect the phosphorylation of VLN2 by activated MPK3 or MPK6 *in vitro* (Supplemental Figure 2C). Sequence alignment of Arabidopsis villins showed that these two phosphosites also exist in VLN4, VLN5, but not in VLN1, VLN2 (Supplemental Figure 2E). However, VLN4 is not required for stomatal defense

(Supplemental Figure 1B). VLN5 is preferentially expressed in pollen tube[15]. When comparing protein sequences between Arabidopsis VLN3 with villin-like proteins from rice, lily and human, these two residues were not conserved in plant and human villins (Supplemental Figure 2E). These data indicate the specific requirement of villin proteins for different cellular processes.

VLN3 phosphorylated by MPK3/MPK6 show enhanced Ca^{2+}-dependent severing activity

The biochemical function of VLN3 has been well-documented previously. It severs actin filaments in Ca^{2+}-dependent manner and bundles actin filaments[14]. To test whether MPK3/MPK6-mediated phosphorylation affects VLN3 activity, we performed high- and low-speed cosedimentation assays and found that phosphorylation modification had no obvious impacts on the filament-binding or bundling activities (Supplemental Figure 3A, B). In the presence of Ca^{2+}, VLN3 decreased the amount of sedimented actin in the reaction, when compared with actin alone. Phosphorylated VLN3 reduced the actin in pellet even further compared to nonphosphorylated VLN3 (Supplemental Figure 3C), suggesting that the filament severing activity of VLN3 was enhanced by the phosphorylation modification.

To confirm the results above, we used total internal reflection fluorescence (TIRF) microscopy to visualize actin dynamics in real time. Prepolymerized oregon-green-labeled actin filaments were adhered to the cover glass of a perfusion chamber as described previously[14]. VLN3 proteins were perfused into the chamber and time-lapse images captured. Analyses with actin without VLN3 showed minimal breakage (Figure 3Aa; Supplemental Figure 4Aa; Supplemental Movie 1). Addition of VLN3 induced breaks along the filaments, demonstrating severing activity (Figure 3Ab; Supplemental Figure 4Ab; Supplemental Movie 2). Phosphorylated VLN3 at the same concentration generated more breaks along the filaments than nonphosphorylated VLN3 (Figure 3Ac; Supplemental Figure 4Ac; Supplemental Movie 3). The number of breaks per unit filament length per unit time (breaks/μm/s) was calculated as a quantitative measure for the severing frequency of each protein. VLN3 exhibited an average severing frequency of 0.0053 breaks/μm/s at 1 nM concentration. The severing was markedly faster when the same amount of VLN3 was phosphorylated (Figure 3B; Supplemental Figure 4B). Actin filament length at steady state was also examined. Prepolymerized actin was incubated with VLN3 in the presence of 10 μM

free Ca^{2+} for 15 min. When incubated without VLN3, actin filaments were on average 20 μm long (Figure 3C; Supplemental Figure 4C). In the presence of VLN3, however, the filaments were significantly shorter, ~7.8 μm in length (Figure 3C; Supplemental Figure 4C). VLN3 phosphorylation reduced filament length to ~3 μm (Figure 3C; Supplemental Figure 4C) and consistent with enhanced filament severing.

Next, we investigated if phosphorylation at Thr777, Ser779 is responsible for enhanced severing activity. We purified recombinant phospho-null (Thr, Ser to Ala) and phosphomimic (Thr, Ser to Asp) VLN3 proteins. Mutating these two residues had no obvious effect on the biochemical properties of VLN3 (Supplemental Figure 5A-C). However, when activated MPK3/MPK6 were added, mutating these two sites abolished the enhanced filament-severing activity of WT VLN3 (Figure 3Ad, B, C; Supplemental Figure 4Ad, B, C; Supplemental Figure 5D, E; Supplemental Movie 4). Taken together, these data demonstrate that MPK3/MPK6-mediated phosphorylation enhances VLN3-induced actin filament severing.

MPK3/MPK6-VLN3 axis is required for actin reorganization during flg22-induced stomatal movement

Actin reorganization is essential for stomatal movement[23–30]. The data above showed that VLN3 phosphorylated by MPK3/MPK6 speed up actin turnover, which might be required for stomatal movement-associated actin remodeling. To test this, we studied whether the reorganization of actin filaments during flg22-induced stomatal closure was altered in *vln3* and *mpk* mutants. The cortical actin array in mock-treated guard cells were measured with metrics described previously[6]. Skewness and density are metrics used to estimate the extent of actin filament bundling and the percentage of occupancy of actin filaments, respectively. The actin arrays in *vln3* guard cells were less bundled, but more abundant than those in WT cells (Figure 4A-C). The *mpk3mpk6* double mutants had similar actin phenotypes to *vln3* mutant, but the defects were more severe (Figure 4A-C). The analyses on actin architecture demonstrate that MPK3/MPK6 and VLN3 are involved in modulating actin organization in guard cells. A more dense and less bundled actin array occurs when MPK3/MPK6 or VLN3 is absent in plant.

The cortical actin array undergoes rearrangement when guard cells were treated with flg22, the actin filaments were radially oriented in open stomata at the beginning of the MAMP treatment. During stomatal closure, a random organized actin

array occurred. In closed stomata, the actin filaments were rearranged and bundled preferentially as long cables in the longitudinal direction (Figure 4D). These actin rearrangements were similar to those observed during ABA-induced or diurnal stomatal movement[24, 31]. In the absence of flg22, WT and *vln3*, *mpk3mpk6* mutant guard cells showed similar actin organizational patterns with radial actin dominating the cell population. Following flg22 treatment for 1 hr, the proportion of WT guard cells with radial actin organization decreased, and actin filaments in the majority of guard cells became randomly or longitudinal distributed. By contrast, the actin networks in most of the *vln3* mutant guard cells stayed as radial and random organization; only about 20% of the guard cells exhibited a longitudinal actin organization. The actin defects in *mpk3mpk6* double mutant were similar to *vln3* mutant (Figure 4E). To confirm these results, the average angles of actin filaments were measured in WT and mutant cells treated with mock or flg22 (Figure 4F). We observed an increase in the average filament angles in flg22-treated WT cells compared to their mock controls, indicating the occurrence of a more longitudinal actin array. There is a slight increase in filament angles in both *vln3* and *mpk3mpk6* mutant treated with mock, when compared with WT cells. However, filament angles failed to increase in mutant cells following MAMP treatment. These data suggest that both VLN3 and MPK3/MPK6 are required for actin rearrangements during flg22-induced stomatal closure.

It has been shown previously that an increase in actin filament abundance in epidermal pavement cells is an early hallmark of PTI[3]. We also tested whether MPK3/MPK6-VLN3 axis is required for actin responses in epidermal pavement cells in response to MAMP. The actin density increases rapidly in WT treated with flg22, and actin array in *vln3* or *mpk3mpk6* mutant showed a WT response, with increased actin density occurring within minutes (Supplemental Figure 6). These data suggest that these proteins are not involved in MAMP-triggered actin remodeling in epidermal pavement cells.

MPK3/MPK6-VLN3 axis regulates actin dynamics in guard cells upon flg22 perception

To gain a deeper insight into the mechanism underlying actin reorganization during stomatal immunity, we explored the actin array dynamics on a macro scale. Using a correlation coefficient analysis that reports the extent of actin array rearrangements over an entire temporal series[32], we showed that actin dynamics became much slower

in WT cells treated with flg22 for 10 min (Figure 5; Supplemental Figure 7). Guard cells of *vln3* or *mpk3mpk6* mutant displayed a less dynamic actin array compared with WT cells, and the actin dynamicity in both mutant cells was less sensitive to flg22 treatment (Figure 5C; Supplemental Figure 7), suggesting that MPK3/MPK6-VLN3 axis contributes to the flg22-induced decrease in actin dynamicity in guard cells.

The correlation coefficient analysis reveals the global changes in actin organization over time, which are influenced by a variety of actin filament behaviors. To better understand how MPK3/MPK6-VLN3 axis modulates actin dynamics, we examined the actin dynamic parameters that are related to the biochemical function of VLN3. In mock-treated cells, loss of VLN3 or MPK3/MPK6 resulted in a significant reduction in bundling frequency, suggesting that actin filaments in *vln3* single mutant and *mpk3mpk6* double mutant were less frequently to form bundles. However, these actin filaments were turned over at a similar rate to WT cells. This explains the more dense and less bundled cortical array in mutant cells. Within minutes, changes in the behaviors of individual actin filaments were observed following flg22 treatment (Figure 6). There was a two-fold decrease in the frequency of bundle formation (Figure 6B). Moreover, the frequency of filament severing was significantly increased by MAMP treatment (Figure 6C). This demonstrates that MAMP treatment destabilizes actin array by decreasing the frequency of bundle formation and increasing the rate of turnover. These combined effects lead to the disruption of radial actin array in the open stomata, which facilitates actin reorganization to initiate stomatal closure. To further confirm whether MPK3/MPK6-VLN3 axis contributes to these dynamic behaviors, we examined these parameters *in vln3-1* and *mpk3mpk6* mutant cells following flg22 treatment. As shown in Figure 6, the changes in filament dynamic behavior induced by MAMP were abrogated in the mutants (Figure 6B, C). Collectively, these data provide genetic evidences that MPK3/MPK6 and VLN3 are required for MAMP-induced actin remodeling in guard cells.

MPK3/MPK6-mediated VLN3 phosphorylation is required for actin dynamics during stomatal defense to bacterial infection

As shown above, MPK3/MPK6 phosphorylate VLN3 to enhance actin turnover *in vitro*. To determine the biological significance of MPK3/MPK6-mediated VLN3 phosphorylation, we generated transgenic plants expressing wild-type VLN3, nonphosphorylatable variant VLN3^{T777A,S779A} and phosphomimetic variant

338 VLN3^{T777D,S779D} under the control of its native promoter in the *vln3-1* mutant
339 background. The dynamicity of actin array was examined in these transgenic plants.
340 In mock-treated cells, both wild-type and mutant VLN3 restored the defects in actin
341 dynamicity of *vln3* mutant to a wild-type level, suggesting that these two residues are
342 not required for VLN3 to regulate actin dynamics *in vivo* under normal conditions
343 (Figure 7; Supplemental Figure 6). When treated with flg22, VLN3^{T777A,S779A} failed to
344 complement the actin phenotype in *vln3* mutant, whereas VLN3 and VLN3^{T777D,S779D}
345 did (Figure 7; Supplemental Figure 6). These data suggest that phosphorylation of
346 VLN3 is required for flg22-indcued changes in actin dynamics during stomatal
347 immunity.
348 We next examined if mutations in VLN3 phosphosites affect stomatal closure
349 in response to flg22. As shown in Figure 8, the *vln3* mutant failed to close stomata
350 after MAMP treatment, whereas the complementary lines carrying WT *VLN3*
351 transgene were fully responsive (Figure 8A). The lines carrying *VLN3^{T777A,S779A}* were
352 less sensitive to flg22. In contrast, flg22-induced stomatal closure was observed in
353 lines carrying *VLN3^{T777D,S779D}* (Figure 8A). Moreover, plant resistance to bacteria were
354 analyzed on these plants. When spray-treated with DC3000, bacteria grew to similar
355 levels on WT and *vln3* complemented with *VLN3*, or *VLN3^{T777D,S779D}*. However, *vln3*
356 plants complemented with *VLN3^{T777A,S779A}* were significantly more susceptible to
357 bacterial infection compared to lines carrying WT and phosphomimic VLN3 (Figure
358 8B). Collectively, these results demonstrate that VLN3 phosphorylation is required for
359 stomatal defense against bacterial infection.
360 We further asked if VLN3 phosphomimic mutants were able to restore the
361 defects in stomatal defense caused by loss of MPK3/MPK6. The WT VLN3,
362 VLN3^{T777A,S779A}, and VLN3^{T777D,S779D} mutants were transformed into the *MPK3SR*,
363 *MPK6SR* plants. The bacteria resistance phenotype was tested for these transgenes.
364 Without NAPP1 treatment, expressing VLN3 or VLN3^{T777D,S779D} led to an enhanced
365 plant resistance to bacterial infection, whereas expressing VLN3^{T777A,S779A} failed to do
366 so (Figure 8C), confirming the requirement of VLN3 phosphorylation for its positive
367 role in plant defense. Moreover, NAPP1-treated *MPK3SR* and *MPK6SR* were more
368 susceptible to spray-inoculated bacteria, which is consistent with previous reports[20].
369 The VLN3^{T777D,S779D} transgene significantly reduced the bacterial population in
370 NAPP1-treated *MPK3SR* and *MPK6SR* plants, whereas the WT VLN3 and

371 VLN3^{T777A,S779A} did not (Figure 8C). These results support that the phosphorylation of
372 VLN3 plays an important role in MPK3/MPK6-mediated stomatal defense.

Discussion

In this study, we demonstrated the role of host actin cytoskeleton to limit bacterial infection on the leaf surface by regulating stomatal immunity. Arabidopsis VLN3-dependent actin organization plays a positive role in this process. Loss of VLN3 fail to activate stomatal immunity to prevent bacterial entry into plants, leading to enhanced plant susceptibility to bacterial infection. Upon flg22 stimulation, VLN3 is rapidly phosphorylated by defense-responsive kinases, MPK3 and MPK6. Two amino acid residues Thr777 and Ser779 are required for VLN3 phosphorylation. This phosphorylation modification significantly enhances the severing activity of VLN3, but has no apparent impacts on other biochemical properties of this protein. Loss of VLN3 or MPK3/MPK6 result in similar actin defects in guard cells. The actin filaments in *vln3* single mutant and *mpk3mpk6* double mutant merge into bundles less frequently than those in WT cells, resulting in a more abundant and less bundled actin array. Additionally, we showed that flg22 induces significant changes in the dynamic behavior of actin filaments in guard cells. MAMP treatment destabilizes actin filaments by decreasing the frequency of bundle formation and increasing the rate of turnover. This leads to the disruption of radial actin array in the open stomata, which facilitates actin reorganization to initiate stomatal closure. These dynamic parameters in *vln3* and *mpk3mpk6* mutant are insensitive to flg22, suggesting that MPK3/MPK6-VLN3 axis is required for actin reorganization during flg22-induced stomatal closure. The functional significance of VLN3 phosphorylation was demonstrated by the findings that phospho-null VLN3 fails to restore the defects in actin dynamics and stomatal defense in *vln3* mutant while wild-type and phosphomimic VLN3 variants do. Collectively, our data demonstrate that VLN3 phosphorylation by MPK3/MPK6 govern actin dynamics to initiate innate immunity gating on host surface.

Consistent with previous phosphoproteomic analyses, we confirmed that VLN3 is rapidly phosphorylated following flg22 activation[9, 10]. Moreover, MPK3/MPK6 is identified as responsible protein kinases for this phosphorylation, and Thr777, Ser779 are critical phosphorylation sites. It has been suggested that VLN3 is a substrate of different protein kinases under various stress conditions[10]. In addition to MPK3/6, Wang et al. (2020) showed that VLN3 is phosphorylated by CKL2, CRLK2, SOS2, SnRK2s, and CPK11 *in vitro*. All of the identified phosphosites of VLN3 are localized in a small region of linker domain, different kinases seem to phosphorylate different sites[9, 10]. This indicates a potential phosphorylation code for the regulation of VLN3 to

mediate different responses triggered by different stresses. Here, we investigated how MPK3/MPK6-induced phosphorylation affects the biochemical activity of VLN3. We showed that the abilities of VLN3 to bind to and bundle actin filaments are not altered by phosphorylation, whereas the Ca^{2+}-dependent severing activity is significantly enhanced. However, it remains unclear how phosphorylation at linker region would have an impact on severing, since this domain predominately mediates actin bundle formation, and the core domain is responsible for the actin-severing properties[33]. Studies have shown that there is an auto-inhibition mechanism in vertebrate villins to prevent actin severing. Tyrosine phosphorylation at the core domain releases the auto-inhibited conformation, promoting the actin-severing activity of villins[34, 35]. This auto-inhibition mechanism may also exist in plant villins. We hypothesize that there might be an association between linker and core domain, which leads to the auto-inhibited conformation of VLN3. Either calcium binding at core domain or phosphorylation at linker region could release this interaction, resulting in a conformational change in villin from an auto-inhibited state to an active state, thus exposing the actin-severing site. However, this hypothesis requires further investigation.

VLN3 and its closest homolog, VLN2, are expressed in all organs and various cell types[17, 18]. Single mutants of these proteins do not show any obvious developmental defects. Actin organization in epidermal cells of single mutants are similar to WT[18]. Loss of both VLN2 and VLN3, however, results in fewer thick bundles and more thin bundles in the cortical actin array, leading to impaired directional organ growth and sclerenchyma development[17, 18]. In this study, we uncovered the function of VLN3 in guard cells. Under untreated condition, actin filaments in *vln3* mutant cells are less frequently merged into bundles, however, they are turned over at a similar rate to WT cells. Consequently, the altered dynamic properties of actin filaments result in a more dense and less bundled cortical array. These data suggest that VLN3 plays a major role in actin bundle formation in guard cells. When stimulated with flg22, the *vln3* mutant fails to close stomata, whereas the single mutant of VLN2 or VLN4 shows a WT response. There is no additive effect in the *vln2vln3* double mutant, suggesting that VLN3 is the dominant villin during stomatal defense. It is well-recognized that the reorganization of actin array in guard cells is important for proper stomatal closure[23–25, 27, 30, 36–38]. However, the mechanism underlying this structural transition remains to be determined. It has been proposed that the destruction of existing actin networks in

open stomata facilitate their closure[37, 39]. Here, we showed that flg22 treatment stimulates changes in actin dynamics within minutes in guard cells, with overall dynamicity of actin array decreases significantly compared to mock treatment. Further quantitative analyses of dynamic changes in the turnover of individual actin filaments have revealed that flg22 treatments destabilize actin array not only by preventing single actin filaments to form bundles, it also triggers faster filament turnover by increasing the frequency of severing, these combined effects contribute to the disassembly of radial actin array in the open stomata and promote stomatal closure. Additionally, our genetic results showed that the actin dynamics fail to respond to MAMP in *vln3* mutant guard cells, demonstrating the requirement of VLN3 for actin disassembly to initiate flg22-induced stomatal closure.

In plant cells, MAMP perception by cell surface receptors result in rapid cellular signaling events that occur on timescales of seconds to minutes, including cytosolic Ca^{2+} fluxes, activation of MAPK and CDPK cascades, and accumulation of ROS and signaling phospholipids. These fast signals could impinge on the actin cytoskeleton by regulating the activity of actin-binding proteins[3]. In this study, we demonstrated that MPK3/MPK6 function upstream of actin cytoskeleton. In guard cells, loss of MPK3/MPK6 reduces the extent of actin filament bundling and increases the filament density. Moreover, actin filaments in the mutants are predominantly longitudinal. During stomatal defense, MPK3/MPK6 is required for the actin structure transition by the rapid disassembly of radial actin array to close stomata. The regulation of actin cytoskeleton by MPK3/MPK6 are mediated by phosphorylation modification on VLN3. *In vitro*, MPK3/MPK6-mediated VLN3 phosphorylation enhances actin turnover. *In vivo*, inhibiting this phosphorylation fails to trigger MAMP-induced actin rearrangements. Moreover, constitutive VLN3 phosphorylation activates stomatal defense in the absence of upstream kinases. We provided genetic evidence that MPK3/MPK6 phosphorylate VLN3 to initiate stomatal immunity by regulating actin dynamics.

Actin networks in different cell types respond distinctly to innate immune activation. In leaf pavement cells or hypocotyl epidermal cells, MAMP treatment increases actin filament abundance and enhances the overall actin array dynamicity[5, 6, 40, 41]. Detailed investigation on dynamic behaviors of actin filaments suggests that MAMP-induced increase in actin filament abundance results from reduced filament disassembly, as well as enhanced availability of dynamic ends for actin polymerization.

In guard cells, however, actin density does not increase and the dynamicity of actin array decreases after MAMP treatment[8, 28]. Moreover, MAMP perception enhances the rate of actin filament turnover. The differences in actin dynamics behaviors between epidermal cells and guard cells demonstrate that the architecture and properties of actin arrays that support different defense responses are highly unique. This is further supported by the findings that, unlike CPK3[8], MPK3/MPK6-VLN3 axis is not involved in actin responses in pavement cells following flg22 perception. In *vln3* or *mpk3mpk6* mutant, actin arrays show WT response to MAMP treatment. These data suggest that innate immune signals impinged on actin cytoskeleton and response regulators vary between different cell types. The repertoire of mechanisms that control actin filament dynamics *in vivo* is more complex than previously appreciated.

Methods

Plant materials and growth conditions

Arabidopsis plants used in this study include Col-0, *vln2-1* (SAIL_813_H02), *vln3-1* (SALK_117097), *vln3-2* (SALK_078340), *vln2vln3*[17, 18], *vln4-1* (SALK_049058), *MPK3SR* line #64 and *MPK6SR* line #58[20]. The plants were grown in the growth room at 23°C at 70% relative humidity with 10/14 hr day/night photoperiod.

To generate VLN3 complementary lines, a native *VLN3* promoter of 2,299 bp in length[18] and cDNA were amplified and cloned into pCAMBIA1300. Desired VLN3 mutant plasmids were generated by site-directed mutagenesis, and the resulting constructs were introduced into *vln3-1* plants by *Agrobacterium*-mediated transformation.

Disease assay

To measure bacterial growth on *Arabidopsis*, 24-day-old leaves were hand infiltrated with bacterial suspensions at 1×10^5 colony-forming units per ml using a needless syringe, or dip inoculated 5×10^5 colony-forming units per ml. Two leaf discs with a diameter of 0.5 cm^2 were collected at 48 hr after infection and ground in 10 mM $MgCl_2$. Following bacterial recovery, serial dilution of leaf extracts was performed. A 2-µl drop from each dilution was plated for counting bacterial colonies. Each data points represents average bacterial numbers from three replicates[5].

For pathogen entry assays, detached leaves were illuminated for 2.5 hr before 1-hr treatment with DC3000 (OD = 0.5). Leaves were washed by 0.02% Silwet L-77 for 10 s. Pathogen entry was measured by direct counting colonies.

Stomatal aperture assay

Leaf peels were collected from the abaxial side of 3 to 4-week-old plant leaves, and incubated in stomata-opening buffer (50 mM KCl, 10 mM $CaCl_2$, and 10 mM MES, pH 6.15) in a growth chamber at 23°C under constant illumination. Stomatal apertures were measured after treatment with mock, 10 µM flg22 or DC3000 (OD = 0.1) for 1 hr using ImageJ software.

Split-luciferase complementation assay

The assay was performed as previously described[42]. To generate constructs of VLN3-Cluc, MPK3-Nluc, MPK6-Nluc, the cDNAs were amplified and cloned into Cluc-pCAMBIA1300 or Nluc-pCAMBIA1300. *Agrobacterium tumefaciens* GV3101 containing the indicated plasmids was infiltrated into expanded leaves of *N. benthamiana* and incubated in the growth room for 48 hr before the LUC activity measurement. For the CCD imaging and LUC activity measurement, 1 mM luciferin was sprayed onto the leaves. The cooled CCD imaging apparatus was used to capture the LUC image. Relative LUC activity per cm^2 infiltrated leaf area was calculated. Each data point contains at least four replicates, and three independent experiments were carried out.

Coimmunoprecipitation assay

The full-length cDNAs of *MPK3* and *MPK6* were cloned into the Flag tag and *VLN3* was cloned into the GFP tag to generate *35S:Flag-MPK3*, *35S:Flag-MPK6* and *35S:GFP-VLN3*. These resulting constructs were infiltrated into *N. benthamiana* via *Agrobacterium*-mediated method. After 48 hr, total proteins were extracted for coIP with the extraction buffer (50 mM HEPES, pH 7.5, 150 mM KCl, 1mM EDTA, 0.5% Triton X-100, 1mM DTT, proteinase inhibitor cocktail), and incubated with anti-Flag agarose beads for 2 hr. Beads were washed five times with washing buffer (50 mM HEPES, pH 7.5, 150 mM KCl, 1mM EDTA, 0.5% Triton X-100, 1mM DTT). After washing, the immunoprecipitated proteins were separated by SDS-PAGE and detected by anti-GFP and anti-Flag immunoblot.

Protein purification

The cDNAs of wild-type, mutated VLN3, its N terminus (719 amino acids) and C terminus (247 amino acids) were cloned into the pGEX-6p-1 vector. The resulting vectors were transformed into *E. coli* (strain BL21). The recombinant proteins were purified with glutathione sepharose.

Phosphorylation assay and phosphosite identification

The *in vitro* phosphorylation assay was performed as described previously[43]. Recombinant His-tagged MPK3 and MPK6 (0.2 μg) were activated by incubation with recombinant His-Flag-tagged $MKK5^{DD}$ (0.05 μg) in the reaction buffer (20 mM Tris-HCl, pH 7.5, 10 mM $MgCl_2$, 50 mM ATP and 1 mM DTT) at 30 °C for 0.5 hr. Activated

MPK3 and MPK6 was then used to phosphorylate recombinant GST-N-VLN3 and GST-C-VLN3 proteins (1:10 enzyme substrate ratio) in the reaction buffer at 30 °C for 30 min. The reactions were stopped by the addition of 5×SDS sample buffer. Proteins were separated in phos-tag gel (10% SDS-PAGE, 50 μM Phos-tag, 100 μM $MnCl_2$). After electrophoresis, the gel was incubated in the transfer buffer (50 mM Tris, 40 mM Glycine) containing 10 mM EDTA three times, and washed in transfer buffer for 10 min, and then transferred to a nitrocellulose membrane, N-VLN3 and C-VLN3 was detected with the anti-GST antibody.

To detect VLN3 phosphorylation in plant, HA-tagged N-VLN3 and C-VLN3 were expressed in Arabidopsis protoplasts. Following treatment with mock or 100 nM flg22 for 10 min, total proteins were extracted with extraction buffer, separated in phos-tag gel and detected by immunoblot analysis.

For phosphosite identification, phosphorylated C-VLN3 by MPK3/MPK6 *in vitro* was excised from SDS-PAGE gel, and in-gel digestion was performed using a well-established protocol with slight modifications[44]. Briefly, the protein embedded in gel slices was reduced with 10 mM DTT and alkylated with 55 mM iodoacetamide, and then digested overnight with sequencing grade trypsin (Sigma) at 37 °C. The tryptic peptides were analyzed by LC-MS/MS using nanoLC-LTQ-Orbitrap XL (ThermoFinnigan). Peptide identification and phosphosites assignment were performed with the Proteome Discoverer software (version 1.4, Thermo Fisher). The *Arabidopsis thaliana* proteome sequences (Uniprot) were used as the database and the mass tolerances were set to 20 PPM for precursor and 0.6 Da for fragment ions for the database search.

Biochemical characterization of phosphorylated VLN3

High-speed and low-speed cosedimentation assays were performed as previously described[33]. Non-phosphorylated or phosphorylated VLN3 were incubated with preformed actin filaments at 1:3 ratio. Individual severing events along actin filaments were imaged by time-lapse TIRF microscopy[45]. The assembly of monomeric actin (Oregon green labeled) was initiated by the addition of one-tenth volume of 10 × KMEI (0.5 mM KCl, 10 mM $MgCl_2$, 10 mM EGTA, 0.1 mM Imidazole, pH 7.0). Actin filaments (15~50% Oregon green-actin, 0.125~1 mM) were mixed with 2 × TIRF buffer (20 mM imidazole [pH 7.4], 100 mM KCl, 2 mM $MgCl_2$, 2 mM EGTA, 0.4 mM ATP, 10 mM DTT,

30 mM glucose, 40 mg/ml catalase, 200 μg/ml glucose oxidase, and 1% methylcellulose) and was transferred to a microscope flow chamber for imaging at room temperature. The VLN3 protein was introduced after placing the chamber on the microscope stage. TIRF images were collected at 1-2 s intervals using ELYRA 7 (Carl Zeiss). Microscope slides (24 × 50 mm 12-545-F; Fisher Scientific) and cover-slips (22 × 22 mm 12-542-B; Fisher Scientific) were cleaned by piranha solution (a 3:1 mixture of sulfuric acid and 30% hydrogen peroxide) overnight. The glass then was incubated with 2 mg/ml methoxy-PEG-silane MW 5000 and 2 mg/ml biotin-PEG-silane MW 3400 (Laysan Bio) in 95% ethanol (pH 2.0) at 70°C. Two parallel strips of double-sided tape were placed on both ends of the coverslip to create a flow chamber.

Quantitative analysis of actin dynamics in guard cells

To visualize actin filaments in plant cells, the *35S:GFP-lifeact* construct was transformed into the wild type, *vln3* mutants, VLN3 complementary lines and *MPK3SR* lines. Guard cells from 3-week-old plants were used for live cell imaging. Actin organization analyses were performed on images acquired with a PerkinElmer UltraView Vox spinning disk microscope equipped with 60×/1.42 Numerical Aperture objective. For time-lapse imaging of actin filament dynamics, the actin array in guard cells was recorded by variable angle epifluorescence microscopy (VEAM) at 1-s intervals, and a series of 100 images were collected. Quantitative analyses of the dynamic behavior of individual actin filaments were performed as described previously[33]. For correlation coefficient analyses, time-lapse VAEM series were cropped and analyzed using the built-in MATLAB function corr2 defined by Vidali and colleagues[5, 32].

References

1. Macho, A.P., Zipfel, C. Plant PRRs and the activation of innate immune signaling. *Mol. Cell* **54**, 263-272 (2014).
2. Li, J., Blanchoin, L., Staiger, C. J. Signaling to actin stochastic dynamics. *Annu. Rev. Plant Biol.* **66**, 415-440 (2015).
3. Li, J., Staiger, C.J. Understanding cytoskeletal dynamics during the plant immune response. *Annu. Rev. Phytopathol*. **56**, 513-533 (2018).
4. Watts, C., Zaru, R., Prescott, A.R., Wallin, R.P., West, M.A. Proximal effects of Toll-like receptor activation in dendritic cells. *Curr. Opin. Immunol.* **19**, 73-78 (2007).
5. Li, J., Henty-Ridilla, J. L., Staiger, B.H., Day, B., Staiger, C.J. Capping protein integrates multiple MAMP signalling pathways to modulate actin dynamics during plant innate immunity. *Nat. Commun.* **6**, 7206 (2015).
6. Li, J., Cao, L., Staiger, C.J. Capping protein modulates actin remodeling in response to reactive oxygen species during plant innate immunity. *Plant Physiol.* **173**, 1125-1136 (2017).
7. Porter, K., Shimono, M., Tian, M., Day, B. Arabidopsis Actin-Depolymerizing Factor-4 links pathogen perception, defense activation and transcription to cytoskeletal dynamics. *PLoS Pathog.* **8**, e1003006 (2012).
8. Lu, Y-J.*,* et al. Arabidopsis calcium-dependent protein kinase 3 regulates actin cytoskeleton organization and immunity. *Nat. Commun.* **11**, 6234 (2020).
9. Rayapuram, N.*,* et al. Identification of novel PAMP-triggered phosphorylation and dephosphorylation events in *Arabidopsis thaliana* by quantitative phosphoproteomic analysis. *J. Proteome Res.* **13**, 2137-2151 (2014).
10. Wang, P.*,* et al. Mapping proteome-wide targets of protein kinases in plant stress responses. *PNAS* **117**, 3270 (2020).
11. Rayapuram, N.*,* et al. Quantitative phosphoproteomic analysis reveals shared and specific targets of Arabidopsis Mitogen-Activated Protein Kinases (MAPKs) MPK3, MPK4, and MPK6. *Mol. Cell. Proteomics* **17**, 61-80 (2018).
12. Huang, S., Qu, X., Zhang, R. Plant villins: Versatile actin regulatory proteins. *J. Integr. Plant Biol.* **57**, 40-49 (2015).
13. Klahre, U., Friederich, E., Kost, B., Louvard, D., Chua, N-H. Villin-like actin-binding proteins are expressed ubiquitously in *Arabidopsis*. *Plant Physiol.* **122**, 35-47 (2000).
14. Khurana, P., Henty, J. L., Huang, S., Staiger, A. M., Blanchoin, L., Staiger, C. J. Arabidopsis VILLIN1 and VILLIN3 have overlapping and distinct activities in bundle formation and turnover. *Plant Cell* **22**, 2727-2748 (2010).
15. Zhang, H.*,* et al. Arabidopsis VILLIN5, an actin filament bundling and severing protein, is necessary for normal pollen tube growth. *Plant Cell* **22**, 2749-2767 (2010).
16. Zhang, Y., Xiao, Y., Du, F., Cao, L., Dong, H., Ren, H. Arabidopsis VILLIN4 is involved in root hair growth through regulating actin organization in a Ca^{2+}-dependent manner. *New Phytol.* **190**, 667-682 (2011).
17. Bao, C.*,* et al. Arabidopsis VILLIN2 and VILLIN3 act redundantly in sclerenchyma development via bundling of actin filaments. *Plant J.* **71**, 962-975 (2012).
18. van der Honing, H. S., Kieft, H., Emons, A. M. C., Ketelaar, T. Arabidopsis VILLIN2 and VILLIN3 are required for the generation of thick actin filament bundles and for directional organ growth. *Plant Physiol.* **158**, 1426-1438 (2012).

19. Melotto, M., Underwood, W., Koczan, J., Nomura, K., He, S. Y. Plant stomata function in innate immunity against bacterial invasion. *Cell* **126**, 969-980 (2006).
20. Su, J.*,* et al. Regulation of stomatal immunity by interdependent functions of a pathogen-responsive MPK3/MPK6 cascade and abscisic acid. *Plant Cell* **29**, 526-542 (2017).
21. Meng, X., Zhang, S. MAPK cascades in plant disease resistance signaling. *Annu. Rev. Phytopathol.* **51**, 245-266 (2013).
22. Berriri, S.*,* et al. Constitutively active mitogen-activated protein kinase versions reveal functions of Arabidopsis MPK4 in pathogen defense signaling. *Plant Cell* **24**, 4281-4293 (2012).
23. Hwang, J.U., Lee, Y. Abscisic acid-induced actin reorganization in guard cells of dayflower is mediated by cytosolic calcium levels and by protein kinase and protein phosphatase activities. *Plant Physiol.* **125**, 2120-2128 (2001).
24. Zhao, Y.*,* et al. The plant-specific actin binding protein SCAB1 stabilizes actin filaments and regulates stomatal movement in *Arabidopsis*. *Plant Cell* **23**, 2314-2330 (2011).
25. Jiang, K., Sorefam, K., Deeks, M. J., Bevan, M. W., Hussey, P. J., Hetherington, A. M. The ARP2/3 complex mediates guard cell actin reorganization and stomatal movement in *Arabidopsis*. *Plant Cell* **24**, 2031-2040 (2012).
26. Li, X.*,* et al. ARP2/3 complex-mediated actin dynamics is required for hydrogen peroxide-induced stomatal closure in *Arabidopsis*. *Plant Cell Environ.* **37**, 1548-1560 (2014).
27. Guo, Y.*,* et al. Casein Kinase1-Like Protein2 regulates actin filament stability and stomatal closure via phosphorylation of actin depolymerizing factor. *Plant Cell* **28**, 1422-1439 (2016).
28. Shimono, M., Higaki, T., Kaku, H., Shibuya, N., Hasezawa, S., Day, B. Quantitative evaluation of stomatal cytoskeletal patterns during the activation of immune signaling in *Arabidopsis thaliana*. *PloS One* **11**, e0159291 (2016).
29. Qian, D.*,* et al. Arabidopsis ADF5 promotes stomatal closure by regulating actin cytoskeleton remodeling in response to ABA and drought stress. *J. Exp. Bot.* **70**, 435-446 (2019).
30. Zheng, W., Jiang, Y., Wang, X., Huang, S., Yuan, M., Guo, Y. AP3M harbors actin filament binding activity that is crucial for vacuole morphology and stomatal closure in *Arabidopsis*. *PNAS* **116**, 18132-18141 (2019).
31. Higaki, T., Kutsuna, N., Sano, T., Kondo, N., Hasezawa, S. Quantification and cluster analysis of actin cytoskeletal structures in plant cells: role of actin bundling in stomatal movement during diurnal cycles in Arabidopsis guard cells. *Plant J.* **61**, 156-165 (2010).
32. Vidali, L., Burkart, G. M., Augustine, R. C., Kerdavid, E., Tüzel, E., Bezanilla, M. Myosin XI is essential for tip growth in *Physcomitrella patens*. *Plant Cell* **22**, 1868-1882 (2010).
33. Zou, M., Ren, H., Li, J. An auxin transport inhibitor targets Villin-mediated actin dynamics to regulate polar auxin transport. *Plant Physiol.* **181**, 161-178 (2019).
34. Zhai, L., Kumar, N., Panebra, A., Zhao, P., Parrill, A. L., Khurana S. Regulation of actin dynamics by tyrosine phosphorylation: Identification of tyrosine phosphorylation sites within the actin-severing domain of villin. *Biochemistry* **41**, 11750-11760 (2002).
35. Kumar, N., Khurana, S. Identification of a functional switch for actin severing by cytoskeletal proteins. *J. Biol. Chem.* **279**, 24915-24918 (2004).

36. Kim, M., Hepler, P. K., Eun, S-O., Ha, K. S., Lee, Y. Actin filaments in mature guard cells are radially distributed and involved in stomatal movement. *Plant Physiol.* **109**, 1077-1084 (1995).
37. Eun, S-O., Lee, Y. Actin filaments of guard cells are reorganized in response to light and abscisic acid. *Plant Physiol.* **115**, 1491-1498 (1997).
38. MacRobbie, E. A. C., Kurup, S. Signalling mechanisms in the regulation of vacuolar ion release in guard cells. *New Phytol.* **175**, 630-640 (2007).
39. Eun, S-O., Lee, Y. Stomatal opening by fusicoccin is accompanied by depolymerization of actin filaments in guard cells. *Planta* **210**, 1014-1017 (2000).
40. Henty-Ridilla, J. L., Shimono, M., Li, J., Chang, J. H., Day, B., Staiger, C. J. The plant actin cytoskeleton responds to signals from microbe-associated molecular patterns. *PLoS Pathog.* **9**, e1003290 (2013).
41. Henty-Ridilla, J. L., Li, J., Day, B., Staiger, C. J. Actin Depolymerizing Factor4 regulates actin dynamics during innate immune signaling in *Arabidopsis*. *Plant Cell* **26**, 340-352 (2014).
42. Li, L., et al. The FLS2-associated kinase BIK1 directly phosphorylates the NADPH oxidase RbohD to control plant immunity. *Cell Host Microbe* **15**, 329-338 (2014).
43. Li, H., et al. MPK3- and MPK6-Mediated ICE1 phosphorylation negatively regulates ICE1 stability and freezing tolerance in *Arabidopsis*. *Dev. Cell* **43**, 630-642.e634 (2017).
44. Shevchenko, A., Tomas, H., Havlis, J., Olsen, J. V., Mann, M. In-gel digestion for mass spectrometric characterization of proteins and proteomes. *Nat. Protoc.* **1**, 2856-2860 (2006).
45. Zhang, S., Liu, C., Wang, J., Ren, Z., Staiger, C. J., Ren, H. A processive Arabidopsis formin modulates actin filament dynamics in association with profilin. *Mol. Plant* **9**, 900-910 (2016).
46. Corpet, F. Multiple sequence alignment with hierarchical clustering. *Nucleic Acids Res.* **16**, 10881-10890 (1988).

Acknowledgments

We thank Dr. Juan Xu (Zhejiang University) for generously providing *MPK3SR* and *MPK6SR* lines. We are grateful to the Experimental Technology Center for Life Sciences, Beijing Normal University for technical support. This research was funded by the Chinese Natural Science Foundation (31801135, 92054101).

Author contributions

M.Z., M.G., and J.L. designed the experiments. M.Z., M.G., Z.Z., B.W., Q.P., and Jiajing.L. performed experiments. M.Z., M.G., J.-M. Z., and J.L. analyzed the data; M.Z., J.-M. Z., and J.L. wrote the paper. All authors commented and agreed on the manuscript before submission.

Competing interests

The authors declare no competing interests.

Figures and figure legends

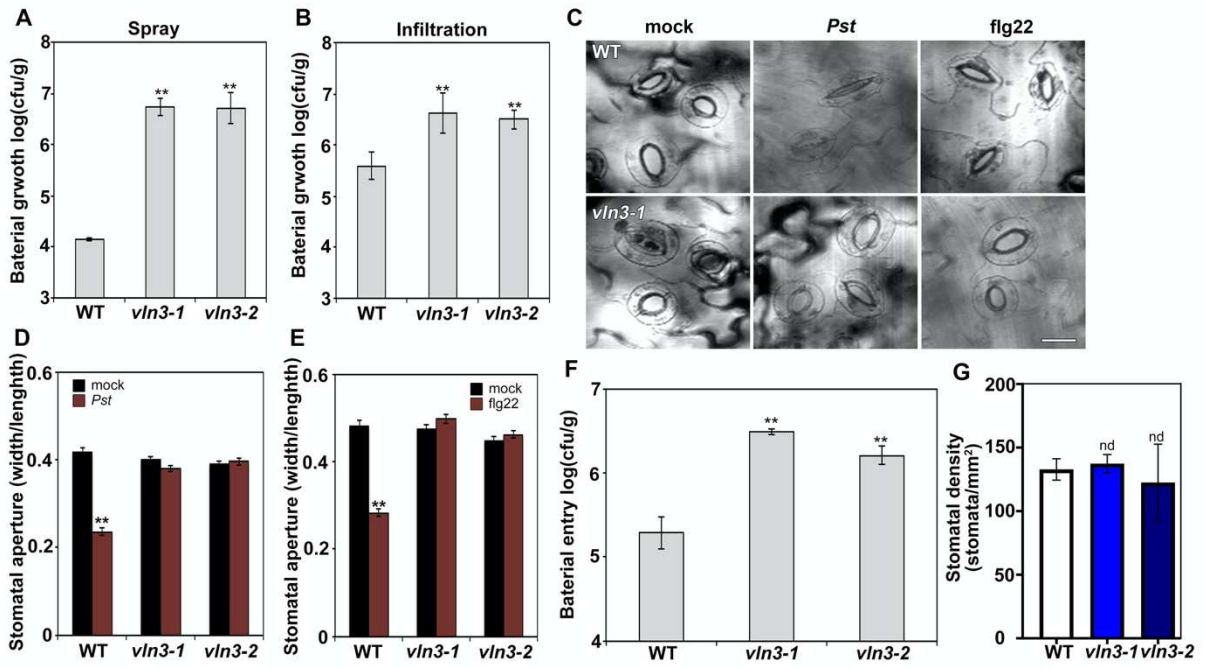

Figure 1. VLN3 plays an essential role in stomatal immunity in *Arabidopsis*.
(A-B) Mutants of VLN3 are more susceptible to bacterial pathogens. Plants of indicated genotypes were sprayed (A) or hand infiltrated (B) with *P. syringae* DC3000. Bacterial growth was measured at 2 d post inoculation (dpi). Representative images of stomatal closure (C) or stomatal aperture measurements (D-E) show impaired pathogen- or MAMP-induced stomatal defense in *vln3* mutants. Scale bar = 20 μm. (F) Loss of VLN3 leads to increased bacteria entry through open stomata. (G) Stomatal density was not altered in *vln3* mutants. Images for stomatal aperture analysis were also used to determine stomatal density. Value are means ± SEM (n=3 for bacterial growth measurements; n>100 stomata from each treatment and genotype were analyzed for stomatal aperture; **P<0.01; nd, no significant difference from WT; Student's *t* test).

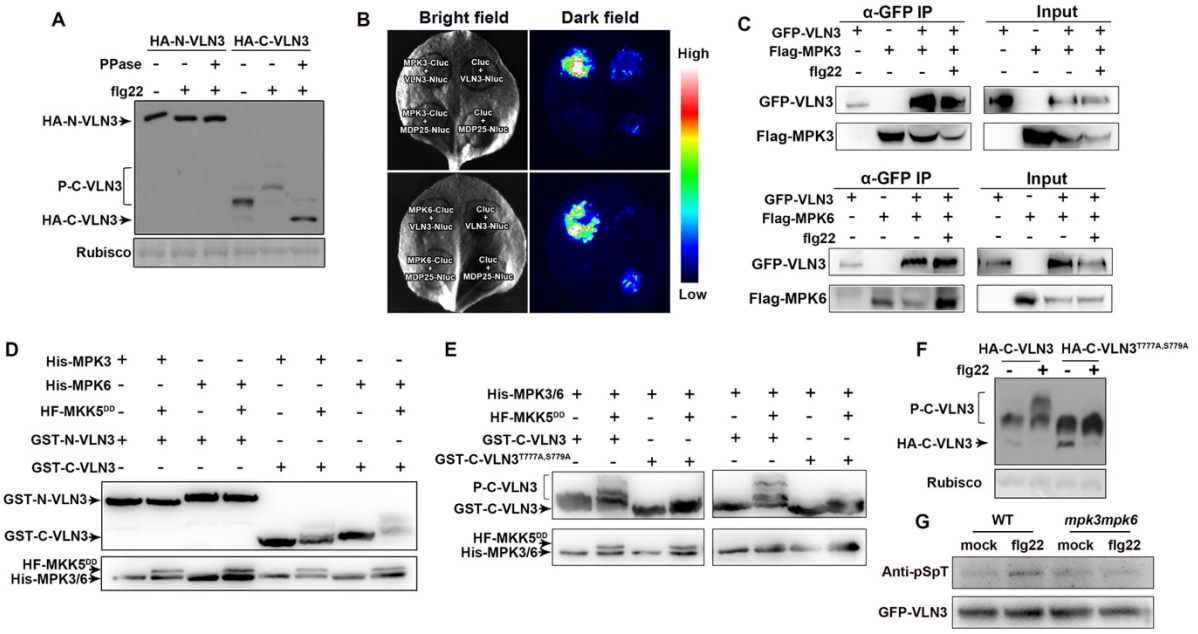

Figure 2. VLN3 is phosphorylated by MPK3/MPK6 during plant innate immunity. (A) The C terminus of VLN3 is phosphorylated *in vivo* upon flg22 activation. HA-tagged N-VLN3 and C-VLN3 were expressed in Arabidopsis protoplasts. Following treatment with mock or 100 nM flg22 for 10 min, total protein was separated in phos-tag gel and VLN3 fragments were detected by anti-HA antibodies. Rubisco was used as a loading control. (B-C) MPK3/MPK6 interact with VLN3 *in vivo*. The indicated constructs were transiently expressed in *N. benthamiana*. Luciferase complementation imaging assay (B) and coIP assay (C) was performed. Nluc, N-terminal fragment of firefly luciferase; Cluc, C-terminal fragment of firefly luciferase. (D) Activated MPK3 and MPK6 phosphorylate C terminus of VLN3 *in vitro*. The N- and C-terminal fragments of VLN3 were incubated with MPK3 or MPK6 in an *in vitro* kinase assay. The phosphorylation of VLN3 was detected in phos-tag gel with anti-GST antibodies. $MKK5^{DD}$ and MPK3/6 was detected in SDS-PAGE using anti-His antibodies. (E-F) Thr777 and Ser779 are required for phosphorylation. Phosphorylation of wild-type and mutated VLN3 was detected *in vitro* (E) by incubation with activated MPK3 (left) or MPK6 (right) or *in vivo* upon flg22 activation (F). (G) MPK3/MPK6 are required for VLN3 phosphorylation *in vivo*. The GFP-VLN3 protein was immunoprecipitated with anti-GFP agarose from *35S:GFP-VLN3 MPK3SR* plants. Before treatment with 10 μM flg22 for 10 min, the *35S:GFP-VLN3 MPK3SR* seedlings were treated with mock or NAPP1 (2.5 μM) for 12 hr. The phosphorylation of VLN3 was detected with immunoblot with anti-phosphoSer/Thr antibodies (pSpT).

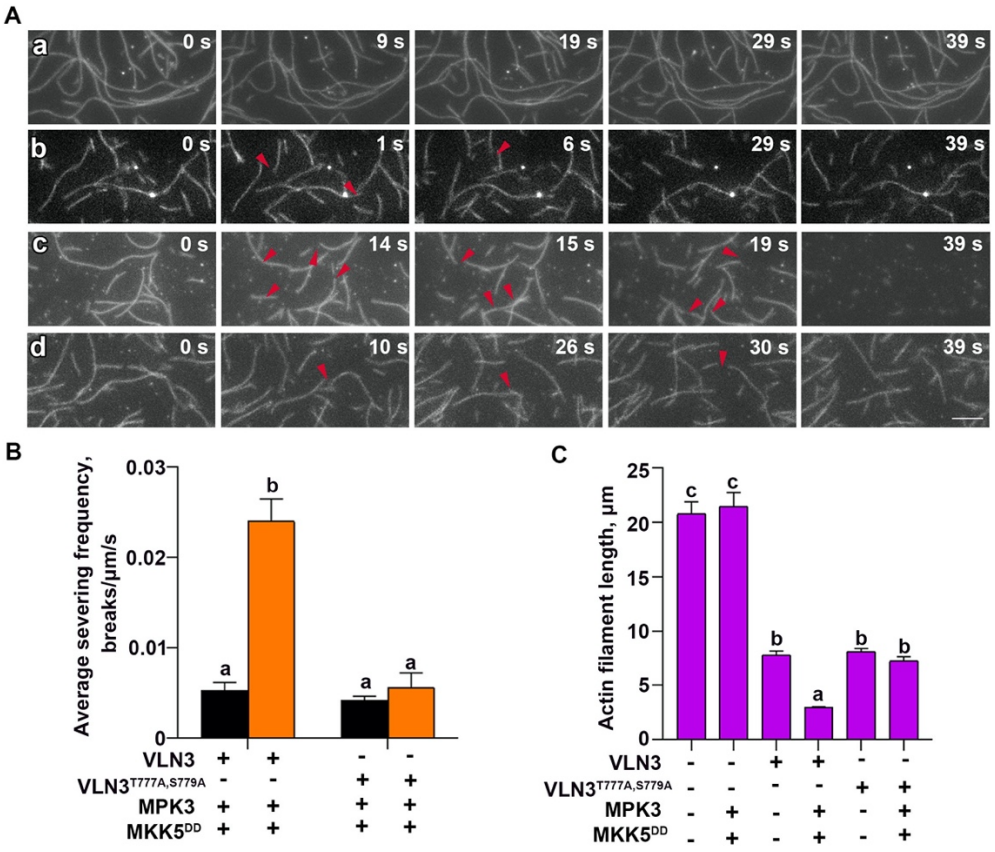

Figure 3. The phosphorylated VLN3 shows enhanced Ca^{2+}-dependent severing activity.

(A) VLN3-mediated actin filament severing was visualized by time-lapse TIRF microscopy. Oregon-green labeled actin filaments were adhered to the cover slip of a perfusion chamber, and then 1 nM wild-type or mutant VLN3 in the presence of 10 μM free Ca^{2+}, was perfused into the chamber and time-lapse images were collected every second. Individual filaments showed breaks (arrows) along their length. The elapsed time in seconds is given in the top right corner of each image (a, actin + MPK3 + $MKK5^{DD}$; b, actin + VLN3; c, actin + VLN3 + MPK3 + $MKK5^{DD}$, d, actin + $VLN3^{T777A,S779A}$ + MPK3 + $MKK5^{DD}$). See also Supplemental Movie 1 to 4 online. Bars = 5 μm. (B-C) Quantitative analysis of severing activity. (B) Severing frequency was calculated as the number of breaks per unit filament length per unit time. At least three independent experiments in which >20 filaments each were counted were performed for each reaction. (C) Average actin filament length was measured for each indicated reaction (n>200 filaments from at least 5 images for each treatment). Value are means ± SEM. Different letters indicate significant differences ($P<0.05$ by Student's *t* test).

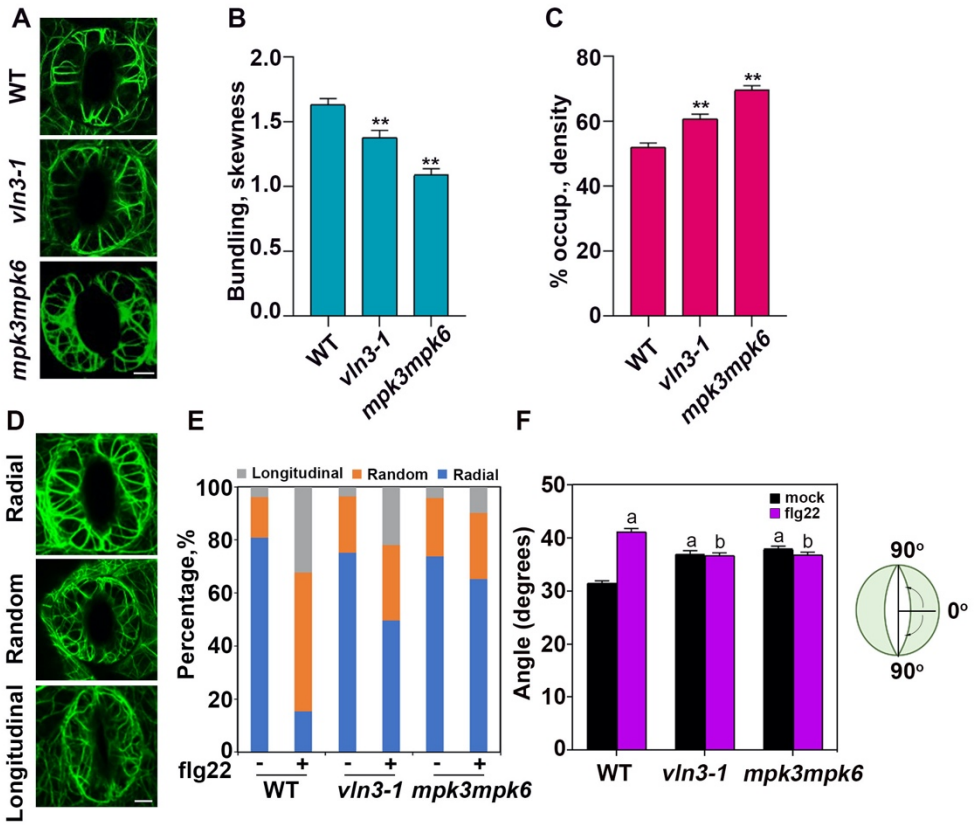

Figure 4. Actin reorganization during MAMP-induced stomatal closure is impaired in *vln3* and *mpk3mpk6* mutants.

(A) Representative images of actin networks in wild-type and mutant guard cells treated with mock. Scale bars = 5 μm. (B) The extent of filament bundling, or skewness, was measured on images collected from guard cells of WT and mutant leaves. (C) Average filament density, or percentage of occupancy, analysis was performed on images used for (B). (D) Representative images of actin networks in wild-type guard cells during MAMP-induced stomatal closure. Actin organization was classified into three groups: radial array, random meshwork; and longitudinal array. Scale bars = 5 μm. Percentage of these groups (E) and actin filaments angles relative to the width of stomatal pore (F) were calculated in indicated genotypes and treatments. Wild-type and *vln3* mutant leaves were treated with 10 μM flg22 for 1 hr. Leaves of *MPK3SR* plants were pretreated with 2 μM NAPP1 for 2 hr prior to flg22 treatment. Value are means ± SEM; At least 100 guard cells per line were measured for each treatment. **P<0.01; a, significantly different from WT treated with mock; b, no significant difference compared to mock control of the same genotype. P<0.01 by Student's *t* test.

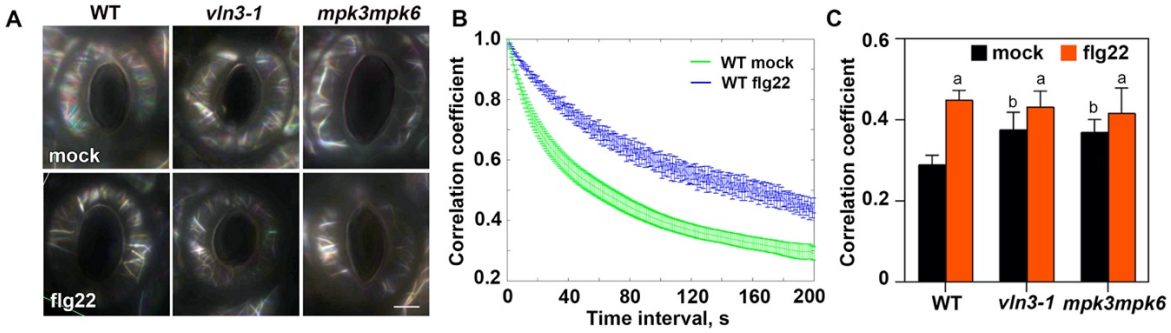

828

829 **Figure 5. Dynamicity of the cortical actin array in WT, *vln3*, *mpk3mpk6* guard**
830 **cells induced by MAMP.**

831 (A) Remodeling of actin array in guard cells were shown in indicated genotypes treated
832 with mock or flg22. Images were merged from three images with 1-min intervals
833 colored in red, green and blue. A white color indicates actin structures that remain
834 relatively stationary during this time period. Scale bar, 5 μm. (B) A correlation
835 coefficient analysis was performed on time-lapse series from WT cells treated with
836 mock, 10 μM flg22 for 10 min. The extent of actin rearrangements, or overall
837 dynamicity of the actin array, was determined by decay in correlation as the temporal
838 interval increased. Lower correlation values correspond with higher dynamicity of the
839 actin array. When compared with mock control, the actin array dynamics were
840 significantly reduced in WT cells treated with MAMP. (C) Values from the last data
841 points of correlation coefficient analyses were shown for each genotype and treatment.
842 Full results of these analyses are shown in Supplemental Figure 7. a, significantly
843 different from mock control of the same genotype; b, significantly different from WT
844 treated with mock; $P<0.001$ by analysis of variance (ANOVA). Analyses were
845 performed on >30 time-lapse series taken from 10 leaves for each treatment and
846 genotype. Error bars represents SEM.

847

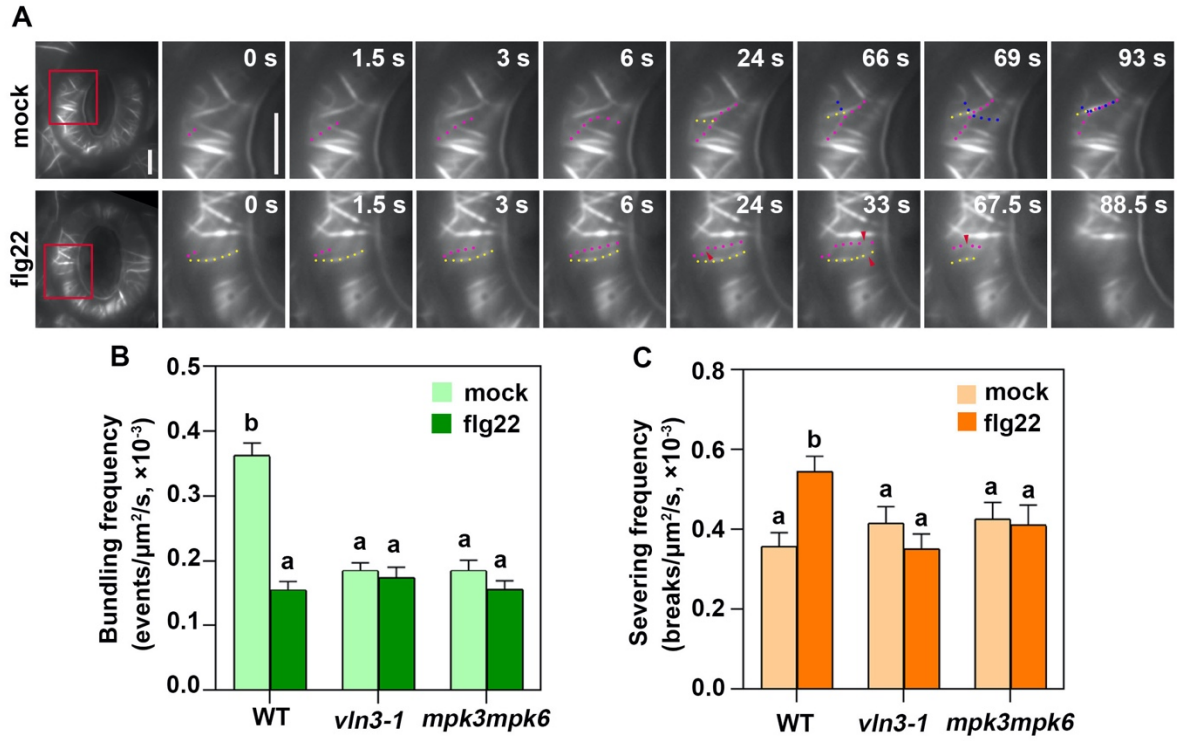

Figure 6. Flg22-induced actin dynamics in WT and mutant guard cells.

(A) Time-lapse images of single actin filaments in WT guard cells treated with mock or 10 μM flg22 for 10 min. In mock-treated cells, single actin filaments (red, yellow and blue dots) touch each other, then bundle by a zippering mechanism (alternating dots). Representative actin filaments (red and yellow dots) from a flg22-treated cell were disassembled by numerous severing events (red arrows). See also Supplemental Movie 5 and 6 online. Scale Bar = 5 μm. Actin filaments in WT cells treated with flg22 showed a significant reduction in bundling frequency (B) and increased severing frequency (C). However, MAMP treatments did not impact any of these parameters in *vln3-1* and *mpk3mpk6* mutant cells. Data are represented as mean ± SEM; different letters indicate significant difference; $P<0.05$ by Student's *t* test. Analyses were performed on 50 regions of interest from 20 time-lapse series taken from 10 leaves for each treatment and genotype.

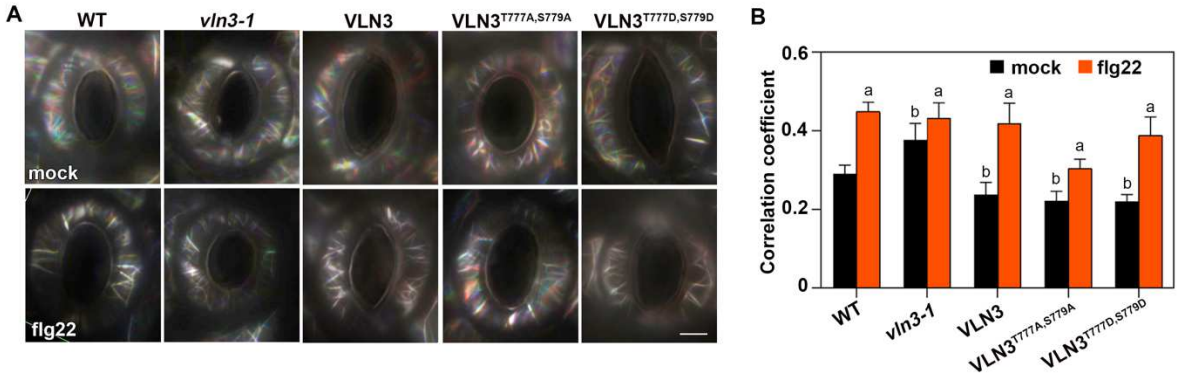

Figure 7. MPK3/MPK6-mediated VLN3 phosphorylation is required for MAMP-induced actin dynamicity in guard cells.

(A) Merged images from time-lapse series were shown in indicated genotypes following mock, 10 μM flg22 treatments for 10 min. Scale bar, 5 μm. (B) Values from the last data points of correlation coefficient analyses are shown for each genotype and treatment. See also Supplemental Figure 7 for full analyses. a, significantly different from mock control of the same genotype; b, significantly different from WT treated with mock; $P<0.001$ by analysis of variance (ANOVA). Analyses were performed on >30 time-lapse series taken from 10 leaves for each treatment and genotype. Error bars represents SEM.

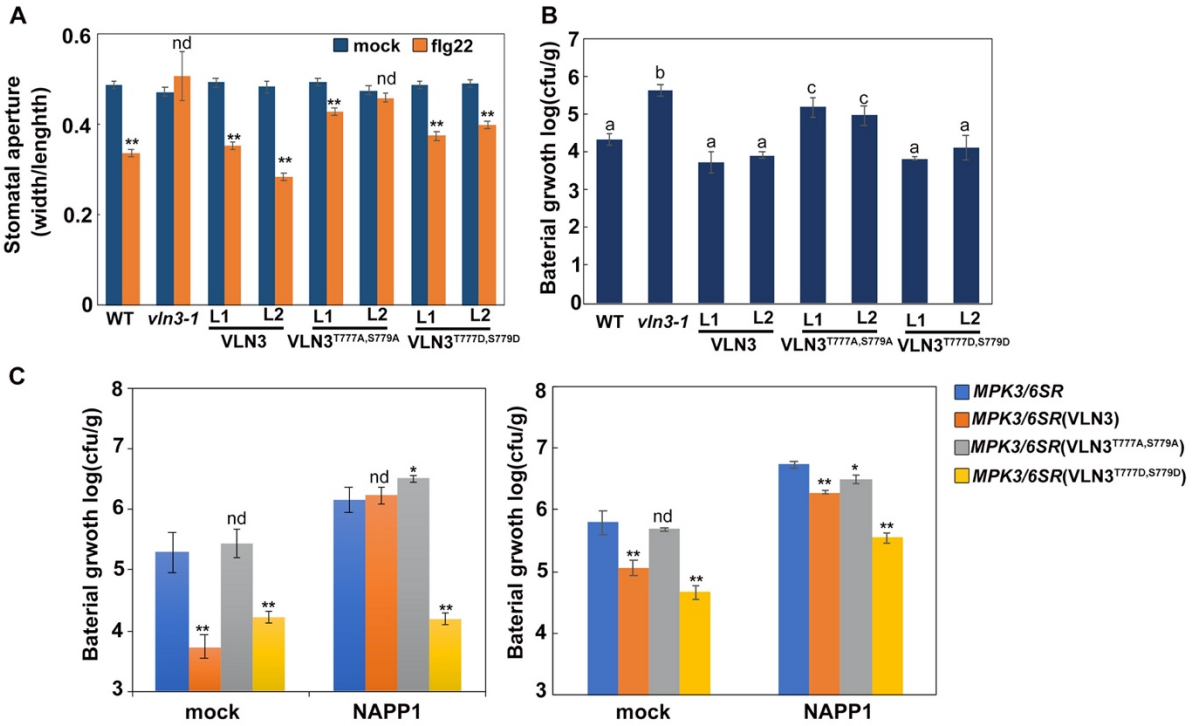

Figure 8. MPK3/MPK6-mediated VLN3 phosphorylation contributes to stomatal defense.

The flg22-induced stomatal closure (A) and bacterial growth (B) was determined on the *vln3* T2 transgenic lines complemented with *VLN3,* $VLN3^{T777A,S779A}$, $VLN3^{T777D,S779D}$. (C) Bacterial growth was determined in the *MPK3SR* (left) or *MPK6SR* (right) overexpressing *VLN3,* $VLN3^{T777A,S779A}$, $VLN3^{T777D,S779D}$. Stomatal apertures were quantified after epidermal peels were treated with flg22 (10 μM) for 1 hr. The bacterial population in the leaf was determined 2 d after plants were spray-inoculated with DC3000. Plants in (C) were pretreated with or without NAPP1 (10 μM) for 3 hr prior to bacterial inoculation. Value are means ± SEM (n=3 for bacterial growth measurements; n>100 stomata from each treatment and genotype were analyzed for stomatal aperture; *P<0.05; **P<0.01 compared with respective mock control; nd, no significant difference; different letters indicate significant difference; P<0.05 by Student's *t* test).

Figures

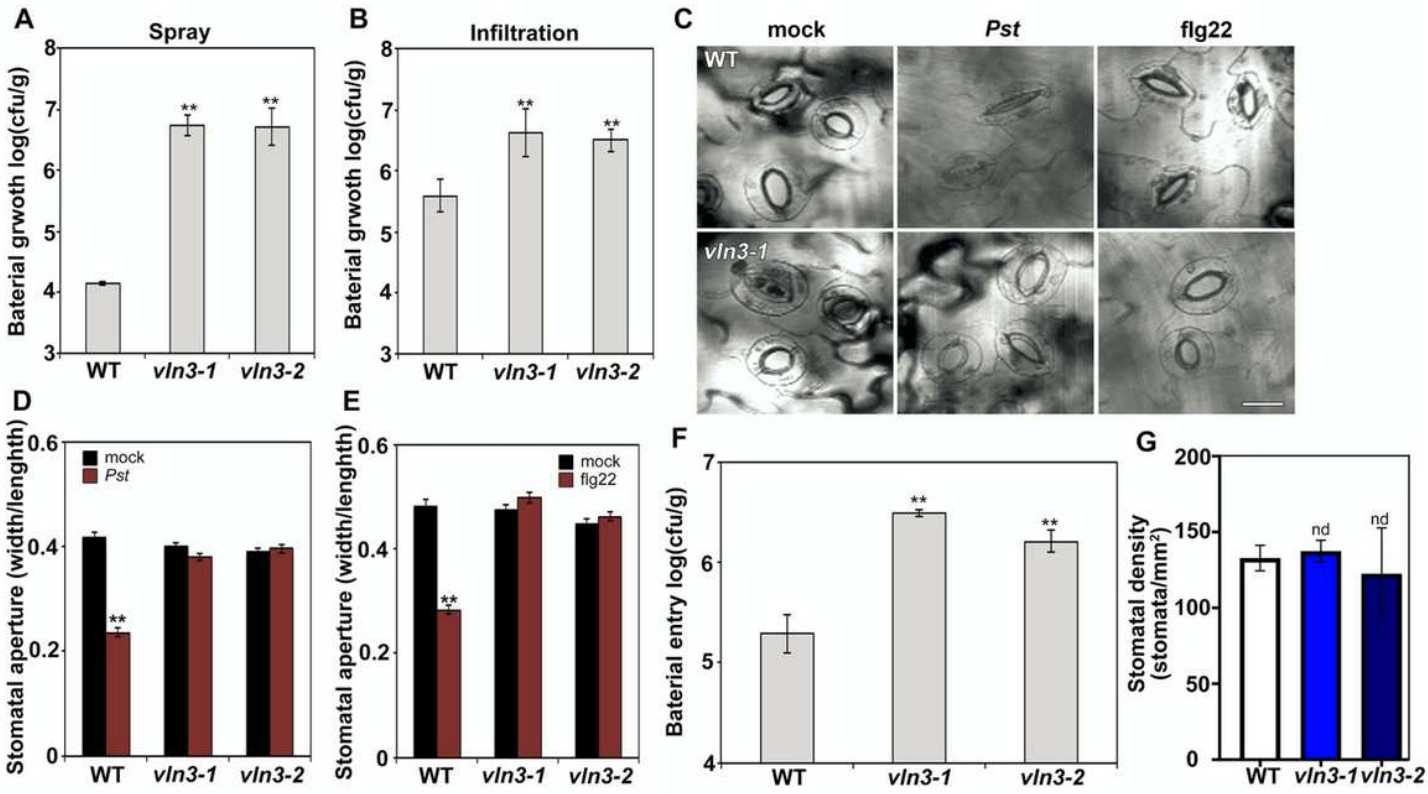

Figure 1

VLN3 plays an essential role in stomatal immunity in Arabidopsis. (A-B) Mutants of VLN3 are more susceptible to bacterial pathogens. Plants of indicated genotypes were sprayed (A) or hand infiltrated (B) with P. syringae DC3000. Bacterial growth was measured at 2 d post inoculation (dpi). Representative images of stomatal closure (C) or stomatal aperture measurements (D-E) show impaired pathogen- or MAMP-induced stomatal defense in vln3 mutants. Scale bar = 20 μm. (F) Loss of VLN3 leads to increased bacteria entry through open stomata. (G) Stomatal density was not altered in vln3 mutants. Images for stomatal aperture analysis were also used to determine stomatal density. Value are means ± SEM (n=3 for bacterial growth measurements; n>100 stomata from each treatment and genotype were analyzed for stomatal aperture; **P<0.01; nd, no significant difference from WT; Student's t test).

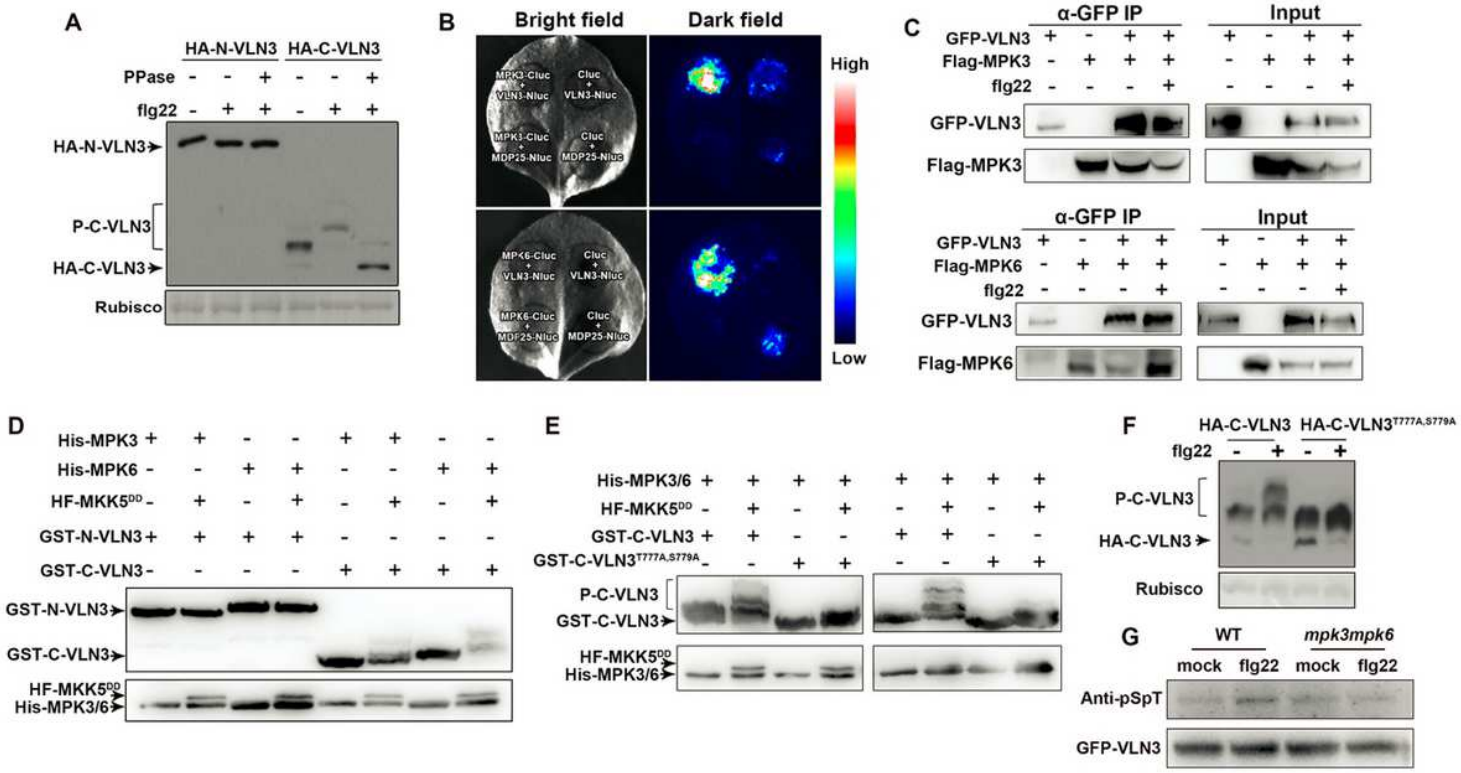

Figure 2

VLN3 is phosphorylated by MPK3/MPK6 during plant innate immunity. (A) The C terminus of VLN3 is phosphorylated in vivo upon flg22 activation. HA-tagged N-VLN3 and C-VLN3 were expressed in Arabidopsis protoplasts. Following treatment with mock or 100 nM flg22 for 10 min, total protein was separated in phos-tag gel and VLN3 fragments were detected by anti-HA antibodies. Rubisco was used as a loading control. (B-C) MPK3/MPK6 interact with VLN3 in vivo. The indicated constructs were transiently expressed in N. benthamiana. Luciferase complementation imaging assay (B) and coIP assay (C) was performed. Nluc, N-terminal fragment of firefly luciferase; Cluc, C-terminal fragment of firefly luciferase. (D) Activated MPK3 and MPK6 phosphorylate C terminus of VLN3 in vitro. The N- and C-terminal fragments of VLN3 were incubated with MPK3 or MPK6 in an in vitro kinase assay. The phosphorylation of VLN3 was detected in phos-tag gel with anti-GST antibodies. MKK5DD and MPK3/6 was detected in SDS-PAGE using anti-His antibodies. (E-F) Thr777 and Ser779 are required for phosphorylation. Phosphorylation of wild-type and mutated VLN3 was detected in vitro (E) by incubation with activated MPK3 (left) or MPK6 (right) or in vivo upon flg22 activation (F). (G) MPK3/MPK6 are required for VLN3 phosphorylation in vivo. The GFP-VLN3 protein was immunoprecipitated with anti-GFP agarose from 35S:GFP-VLN3 MPK3SR plants. Before treatment with 10 μM flg22 for 10 min, the 35S:GFP-VLN3 MPK3SR seedlings were treated with mock or NAPP1 (2.5 μM) for 12 hr. The phosphorylation of VLN3 was detected with immunoblot with anti790 phosphoSer/Thr antibodies (pSpT).

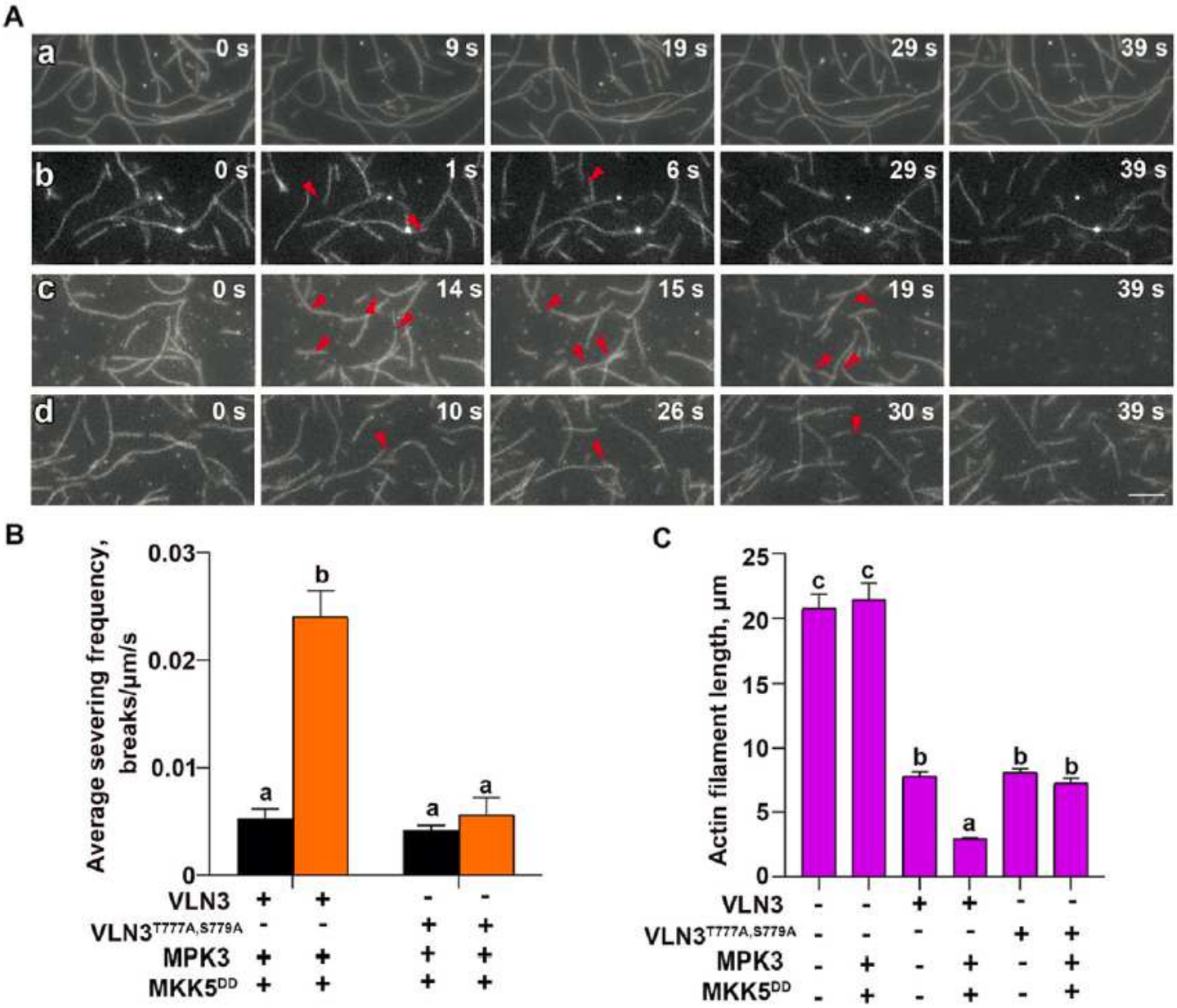

Figure 3

The phosphorylated VLN3 shows enhanced Ca2+-dependent severing activity. (A) VLN3-mediated actin filament severing was visualized by time-lapse TIRF microscopy. Oregon-green labeled actin filaments were adhered to the cover slip of a perfusion chamber, and then 1 nM wild-type or mutant VLN3 in the presence of 10 μM free Ca2+, was perfused into the chamber and time-lapse images were collected every second. Individual filaments showed breaks (arrows) along their length. The elapsed time in seconds is given in the top right corner of each image (a, actin + MPK3 + MKK5DD; b, actin + VLN3; c, actin + VLN3 + MPK3 + MKK5DD, d, actin + VLN3T777A,S779A + MPK3 + MKK5DD). See also Supplemental Movie 1 to 4 online. Bars = 5 μm. (B-C) Quantitative analysis of severing activity. (B) Severing frequency was calculated as the number of breaks per unit filament length per unit time. At least three independent experiments in which >20 filaments each were counted were performed for each reaction. (C) Average

actin filament length was measured for each indicated reaction (n>200 filaments from at least 5 images for each treatment). Value are means ± SEM. Different letters indicate significant differences (P<0.05 by Student's t test).

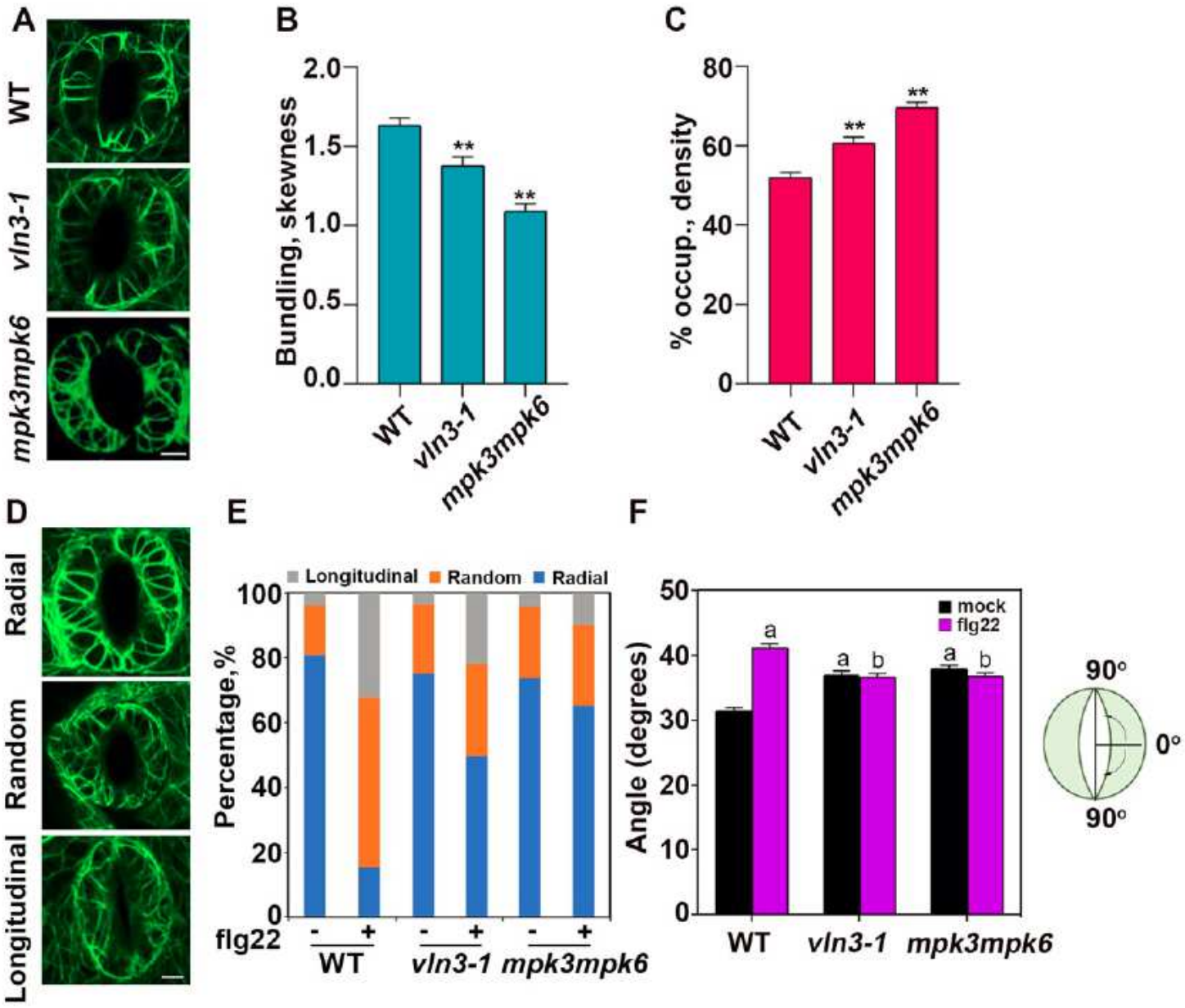

Figure 4

Actin reorganization during MAMP-induced stomatal closure is impaired in vln3 and mpk3mpk6 mutants. (A) Representative images of actin networks in wild-type and mutant guard cells treated with mock. Scale bars = 5 μm. (B) The extent of filament bundling, or skewness, was measured on images collected from guard cells of WT and mutant leaves. (C) Average filament density, or percentage of occupancy, analysis was performed on images used for (B). (D) Representative images of actin networks in wild-type guard cells during MAMP-induced stomatal closure. Actin organization was classified into three groups: radial array, random meshwork; and longitudinal array. Scale bars = 5 μm. Percentage of these groups (E) and

actin filaments angles relative to the width of stomatal pore (F) were calculated in indicated genotypes and treatments. Wild-type and vln3 mutant leaves were treated with 10 μM flg22 for 1 hr. Leaves of MPK3SR plants were pretreated with 2 μM NAPP1 for 2 hr prior to flg22 treatment. Value are means ± SEM; At least 100 guard cells per line were measured for each treatment. **P<0.01; a, significantly different from WT treated with mock; b, no significant difference compared to mock control of the same genotype. P<0.01 by Student's t test.

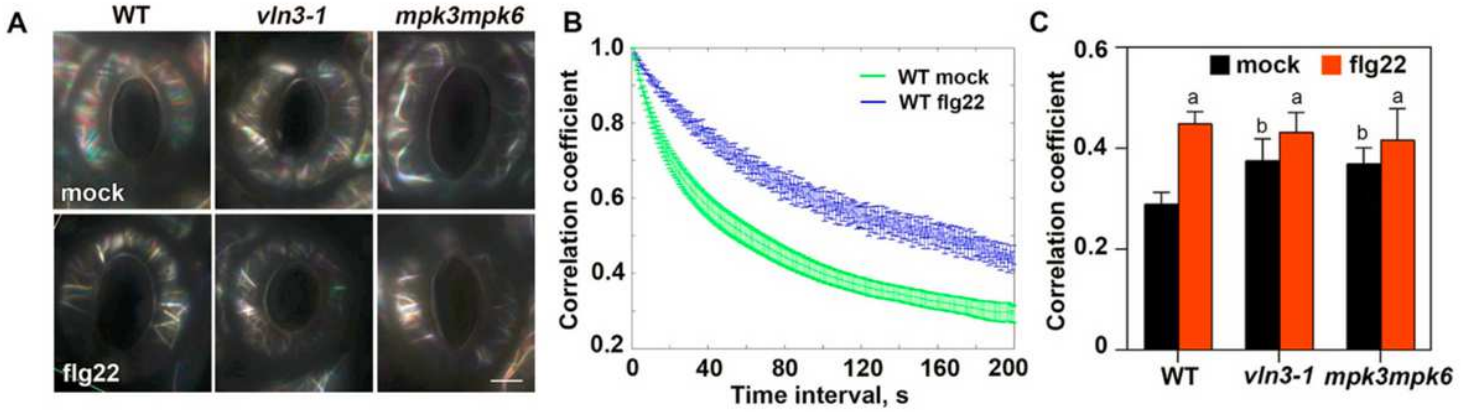

Figure 5

Dynamicity of the cortical actin array in WT, vln3, mpk3mpk6 guard cells induced by MAMP. (A) Remodeling of actin array in guard cells were shown in indicated genotypes treated with mock or flg22. Images were merged from three images with 1-min intervals colored in red, green and blue. A white color indicates actin structures that remain relatively stationary during this time period. Scale bar, 5 μm. (B) A correlation coefficient analysis was performed on time-lapse series from WT cells treated with mock, 10 μM flg22 for 10 min. The extent of actin rearrangements, or overall dynamicity of the actin array, was determined by decay in correlation as the temporal interval increased. Lower correlation values correspond with higher dynamicity of the actin array. When compared with mock control, the actin array dynamics were significantly reduced in WT cells treated with MAMP. (C) Values from the last data points of correlation coefficient analyses were shown for each genotype and treatment. Full results of these analyses are shown in Supplemental Figure 7. a, significantly different from mock control of the same genotype; b, significantly different from WT treated with mock; P<0.001 by analysis of variance (ANOVA). Analyses were performed on >30 time-lapse series taken from 10 leaves for each treatment and genotype. Error bars represents SEM.

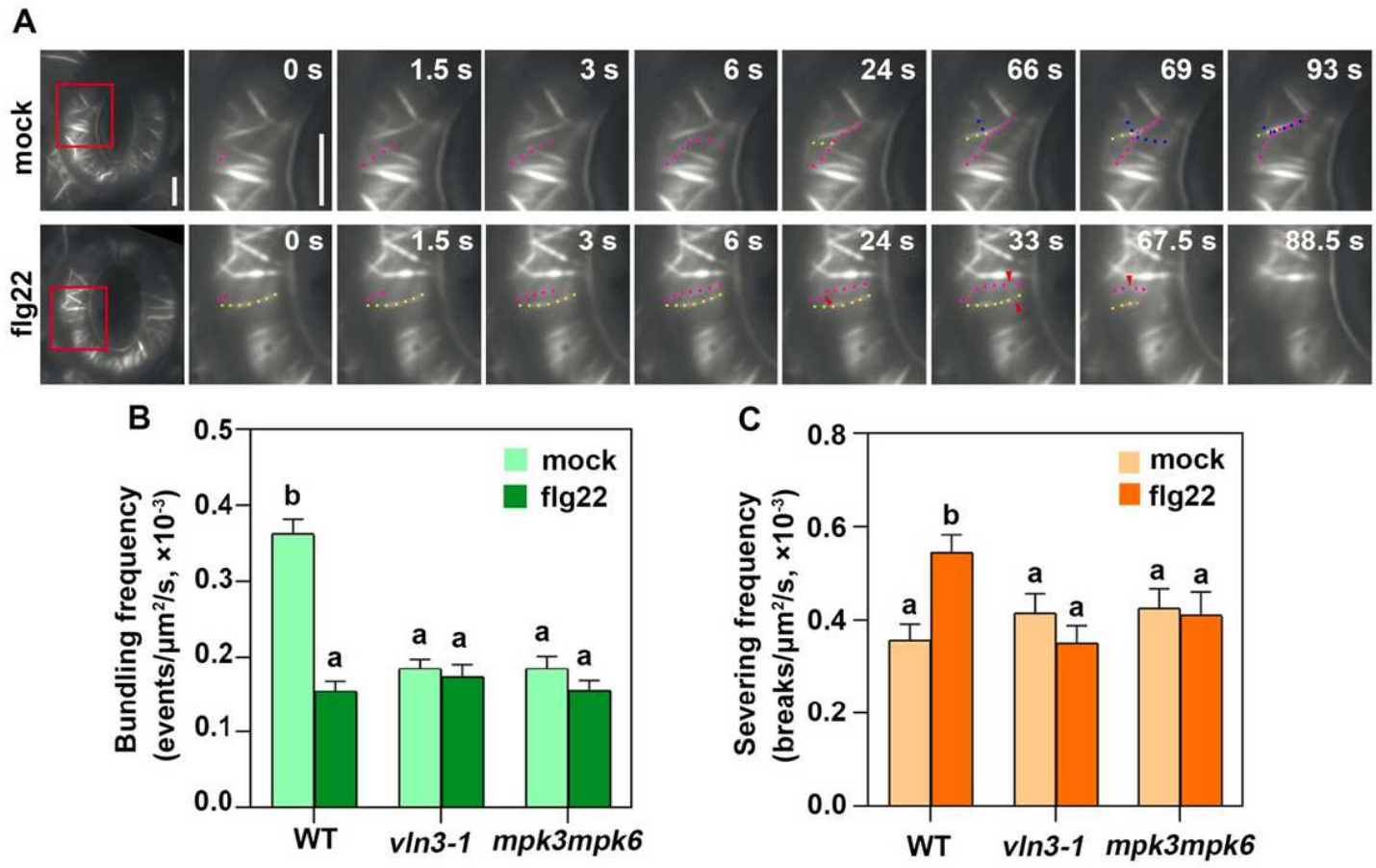

Figure 6

Flg22-induced actin dynamics in WT and mutant guard cells. (A) Time-lapse images of single actin filaments in WT guard cells treated with mock or 10 μM flg22 for 10 min. In mock-treated cells, single actin filaments (red, yellow and blue dots) touch each other, then bundle by a zippering mechanism (alternating dots). Representative actin filaments (red and yellow dots) from a flg22-treated cell were disassembled by numerous severing events (red arrows). See also Supplemental Movie 5 and 6 online. Scale Bar = 5 μm. Actin filaments in WT cells treated with flg22 showed a significant reduction in bundling frequency (B) and increased severing frequency (C). However, MAMP treatments did not impact any of these parameters in vln3-1 and mpk3mpk6 mutant cells. Data are represented as mean ± SEM; different letters indicate significant difference; $P<0.05$ by Student's t test. Analyses were performed on 50 regions of interest from 20 time-lapse series taken from 10 leaves for each treatment and genotype.

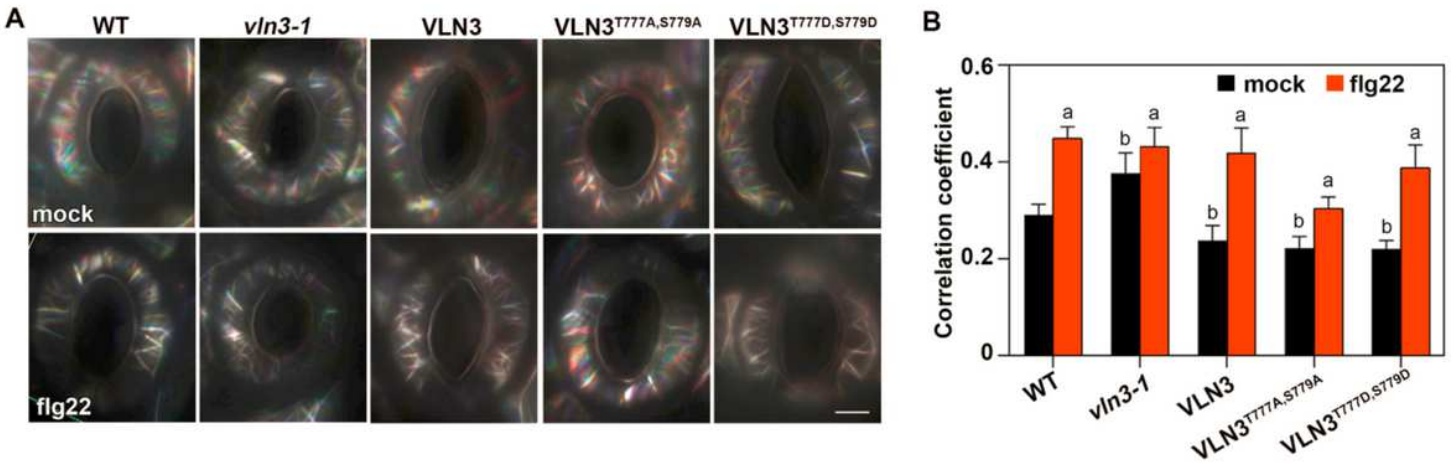

Figure 7

MPK3/MPK6-mediated VLN3 phosphorylation is required for MAMP induced actin dynamicity in guard cells. (A) Merged images from time-lapse series were shown in indicated genotypes following mock, 10 μM flg22 treatments for 10 min. Scale bar, 5 μm. (B) Values from the last data points of correlation coefficient analyses are shown for each genotype and treatment. See also Supplemental Figure 7 for full analyses. a, significantly different from mock control of the same genotype; b, significantly different from WT treated with mock; P<0.001 by analysis of variance (ANOVA). Analyses were performed on >30 time-lapse series taken from 10 leaves for each treatment and genotype. Error bars represents SEM.

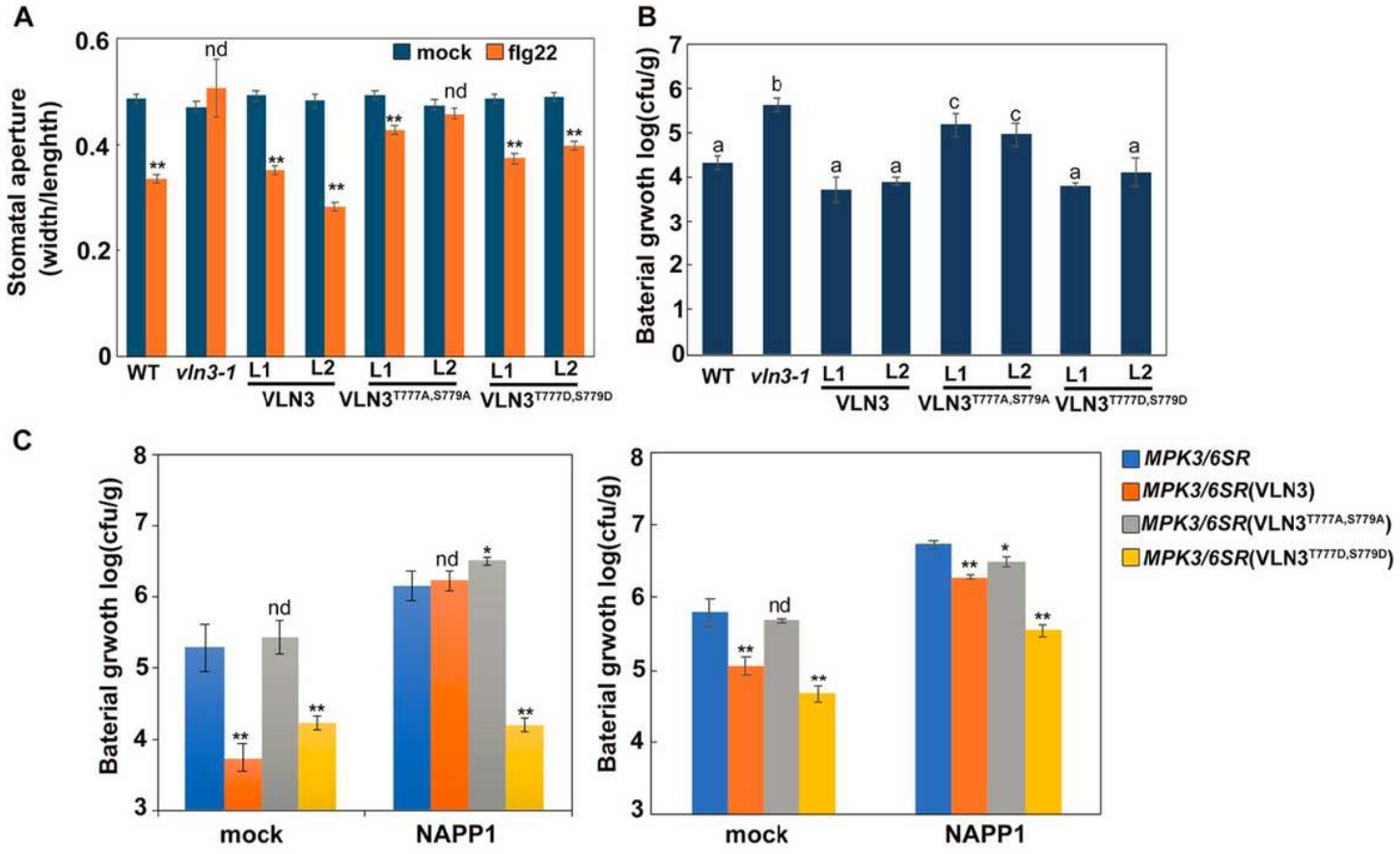

Figure 8

MPK3/MPK6-mediated VLN3 phosphorylation contributes to stomatal defense. The flg22-induced stomatal closure (A) and bacterial growth (B) was determined on the vln3 T2 transgenic lines complemented with VLN3, VLN3T777A,S779A, VLN3T777D,S779D. (C) Bacterial growth was determined in the MPK3SR (left) or MPK6SR (right) overexpressing VLN3, VLN3T777A,S779A, VLN3T777D,S779D. Stomatal apertures were quantified after epidermal peels were treated with flg22 (10 μM) for 1 hr. The bacterial population in the leaf was determined 2 d after plants were spray inoculated with DC3000. Plants in (C) were pretreated with or without NAPP1 (10 μM) for 3 hr prior to bacterial inoculation. Value are means ± SEM (n=3 for bacterial growth measurements; n>100 stomata from each treatment and genotype were analyzed for stomatal aperture; *P<0.05; **P<0.01 compared with respective mock control; nd, no significant difference; different letters indicate significant difference; P<0.05 by Student's t test).

Supplementary Files

This is a list of supplementary files associated with this preprint. Click to download.

- Supplementaryinformation.pdf
- Supplementalmovie1.mp4
- Supplementalmovie2.mp4
- Supplementalmovie3.mp4
- Supplementalmovie4.mp4
- Supplementalmovie5.mp4
- Supplementalmovie6.mp4